Numerical simulation of film cooling applicable to Gas Turbine blades

A Thesis Submitted
in Partial Fulfillment of the Requirements
for the Degree of
Master of Technology

by
Revelli Mahesh Kumar

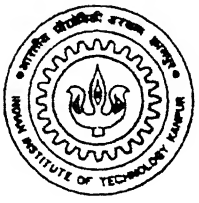

to the
Department of Mechanical Engineering
Indian Institute of Technology, Kanpur
May, 1998

ME- 1998 - M- KUM- NUM

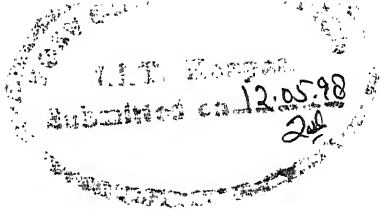

Certificate

It is certified that the work contained in the thesis entitled "*Numerical simulation of film cooling applicable to Gas-Turbine blades*" by Mr. *Revelli Mahesh Kumar*, has been carried out under our supervision and that this has not been submitted elsewhere for a degree.

Subrata Sarkar.

(Dr Subrata Sarkar)
Assistant Professor,
Dept. of Mechanical Engineering,
Indian Institute of Technology,
Kanpur - 208016.

Gautam Biswas

(Dr Gautam Biswas)
Professor,
Dept. of Mechanical Engineering,
Indian Institute of Technology,
Kanpur - 208016.

May, 1998

Dedicated to my beloved Parents

Acknowledgements

I am extremely greatful to Prof. S. Sarkar and Prof. G. Biswas for their extremely valuable guidance and constructive critisism throughout the present work. I am also thankful to them for providing me all kinds of computer facilities, without which my work would have been impossible.

I am also thankful to Prof. S.Sarkar for his esteemed source of inspiration given to me and I shall be indebted to him for ever.

I would like to express my thanks to all my friends, who helped me in preparing the thesis report. Especially I am indebted to my friends csreddy, dreddy, manil, breddy, kjeevan, kosiva, koduri, bsuresh, ksat, yarram, kaku and Guptaji for their help in getting my thesis prepared in time.

I feel happy to express my thanks to my friends Debasish and Kaushik for their timely help during my defence.

I would like to convey my thanks to all my friends who helped me directly or indirectly during my memorable stay at Hall-4, I. I. T. Kanpur.

Mahesh Kumar

CONTENTS

ABSTRACT

The major contributing factor towards the development of modern aeroengines is use of a high gas entry temperature. Thus, an intensive cooling of turbine blades is essential. Film cooling using discrete jets in conjunction with the internal convective cooling are often deployed to keep the blade temperature under the metallurgical limit. The art of blade cooling has established itself as a very important subject in aerospace industries. The successful implementation of blade cooling guarantees the long life of an aeroengine. The determination of optimal configuration of the turbine blade cooling requires extreme care which calls for highly accurate computational methods. The flow field near the coolant holes is very complex due to the interaction of coolant jets with the hot cross flow. The aero-thermal behaviour of the flow depends on a large number of parameters such as coolant emission geometry, blowing ratio, density ratio and free stream conditions.

The present study aims to illustrate the variation of complex aerodynamics and heat transfer phenomena which occurs in a jet-cross flow interaction with the changes in injection angle, blowing ratio and jet exit velocity profile. The time dependent mass averaged three-dimensional compressible Navier-Stokes equations are solved based on finite volume formulation. The explicit second order accurate, cell centered, time-split algorithm of MacCormack is used. Even on the modern computational platforms, the numerical simulation of film cooling applied to turbine blades needs a considerable CPU time. Thus, the present study is limited to the film cooling on a flat plate, which meaningfully illustrates the physics of jet-cross flow interaction. Admittedly, effects of rotation and surface curvature are absent in this analysis. The turbulence is simulated by the algebraic Baldwin-Lomax model. It is worth examining the performance of the Baldwin-Lomax model for this particular simulation, considering both simplicity and economy of computation. The Baldwin-Lomax model is modified with a relaxation technique in an attempt to account for the upstream turbulence history. It is worth noting that the Baldwin-Lomax model is capable to capture the complex flow physics reasonably well. The inclusion of relaxation technique improves the accuracy of the predictive procedure.

NOMENCLATURE

c	Speed of sound
c_f	Skin friction coefficient
c_p	Specific heat at constant pressure
c_v	Specific heat at constant volume
D	Diameter of hole
DR	Density ration (ρs/ρd)
e	Total energy per unit mass
E	x term of flux vector Q
F	y term of flux vector Q
G	z term of flux vector Q
H	Source terms vector
k	Thermal conductivity
l	Turbulence length scale
M	Mach Number
m	Blowing ratio $\left(\frac{\rho_s V_s}{\rho_\infty V_\infty}\right)$
$\dot{m}$	Coolant mass flow rate
Nu	Nusselt Number
p	Pressure

Pr	Prandtl number (0.7 for air)
Pr_t	Turbulent Prandtl number (0.9)
q_i	Heat flux vector
R_x	Gas constant
$\bar{r}$	Position vector
Re	Reynolds number $\left(\frac{\rho UD}{\mu}\right)$
$\bar{S}$	Surface normal Vector
T	Temperature
U	Solution vector
u,v,w	Velocity components
u_τ	Friction velocity = $\sqrt{\frac{\tau_w}{\rho_w}}$
V	Velocity vector
x,y,z	Cartesian co-ordinates
Y^+	Law-of-the Wall Co-ordinate

Greek Symbols

α	Injection angle
γ	Ratio of specific heats (C_p/C_v)
δ	Boundary layer thickness

Pr	Prandtl number (0.7 for air)
Pr_t	Turbulent Prandtl number (0.9)
q_i	Heat flux vector
R_x	Gas constant
$\bar{r}$	Position vector
Re	Reynolds number $\left(\frac{\rho UD}{\mu}\right)$
$\bar{S}$	Surface normal Vector
T	Temperature
U	Solution vector
u,v,w	Velocity components
u_τ	Friction velocity = $\sqrt{\frac{\tau_w}{\rho_w}}$
V	Velocity vector
x,y,z	Cartesian co-ordinates
Y^+	Law-of-the Wall Co-ordinate

Greek Symbols

α	Injection angle
γ	Ratio of specific heats (C_p/C_v)
δ	Boundary layer thickness

Δ	Small increment
δ_{ij}	Kronecker delta
λ	Relaxation length scale
η	Adiabatic film cooling effectiveness $\left[\frac{(T_{aw} - T_r)}{(T_{2r} - Tr)}\right]$
ζ, η, ξ	Curvilinear coodinates
μ	Molecular coefficient of viscosity
μ_t	Turbulent coefficient of viscosity
ν	Kinematic viscosity
ρ	Density
τ_{ij}	Stress tensor
Ω	Cell volume
Δt	Time step
ω	Vorticity
BL	Baldwin-Lomax Model

Subscript

0	Stagnation conditions
1	Inlet plane
2	Exit plane
aw	Adiabatic wall conditions
is	Inentropic condition
i,j,k	Cell indices in x,y,z directions respectively

max	maximum
min	minimum
r	Mainstream recovery condition
s	Secondary fluid condition
t	turbulent
w	wall condition
θ	Momentum thickness
∞	Free stream condition

Superscripts

n	Present time level
'	Fluctuating quantity in density-weighted

LIST OF FIGURES

Chapter 1

INTRODUCTION

1.1 GENERAL

Quite a few components of the gas turbines used in modern aircrafts, operate in extremely harsh environment where the ambient temperature routinely exceeds the melting point of available alloys. The materials that are usually available cannot stand temperatures in excess of 1300 K. The need to protect/cool the solid surfaces exposed to high temperature is an important task. At the same time, the maximum temperature of the cycle can be increased by cooling such surfaces. Incorporation of various cooling techniques and development of new materials have brought about tremendous increase in turbine inlet temperature. Today, the commercial aircraft engines operate with the maximum cycle temperature in excess of 1600K.

Various cooling methods concerning the turbine components have emerged during last twenty five years. The most useful method is to introduce a secondary fluid into the boundary layer on the surface to be cooled/protected. The various means of introducing this secondary fluid into the boundary layer include ablation, transpiration and film cooling. In ablation cooling, an added coating or heat shield decomposes due to sublimation and other highly endothermic processes. As a result a significant quantity of gas enters into the boundary layer. In transpiration cooling, the surface is usually made of porous material and the secondary fluid enters the boundary layer through this permeable surface.

Both ablation and transpiration cooling are primarily designed to protect the region where the secondary fluid enters the boundary layer. They are highly effective since a considerable portion of the heat flux towards the wall can be taken up by the injected coolant where the heat load is the highest. In addition, the gas entering the boundary layer effectively thickens it, and the heat transfer rate is decreased. These two methods, however, do suffer from some disadvantages which preclude their use in many applications. The ablating material is not in general renewable and so ablation cooling has been restricted to systems with high heat fluxes of short duration. Examples are re-entry vehicles. This restriction does not apply to transpiration cooling since a coolant can be continuously introduced through the porous surface. However, the porous materials usually do not possess high mechanical strength which is essential for certain applications like rotor blades of the turbines. Also, small pore size often leads to clogging and a resulting maldistribution of the coolant flow.

In film cooling, albeit a secondary fluid is added to the boundary layer, there exist considerable differences in operation and even in goals as compared to ablation and transpiration cooling. The fundamental difference is that the film cooling is not primarily intended to protect the surface just at the location of coolant addition. Rather it protects the region downstream of the injection location. Film cooling is thus the introduction of a secondary fluid (coolant or injected fluid) at one or more descrete locations on a surface exposed to a high temperature environment. The surface covered with a thin film of cool air is not only in the immediate region of injection but also in the downstream region. The interaction of the coolant jets with the hot mainstream is illustrated in Fig. 1.

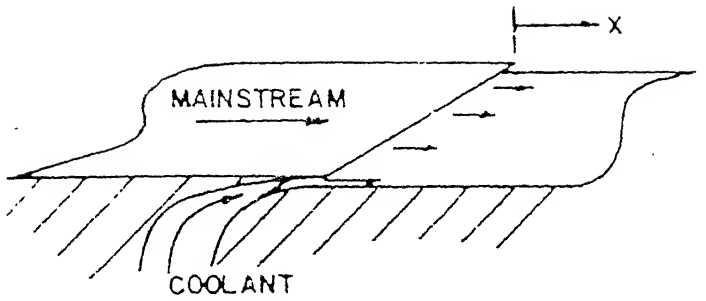

(a)

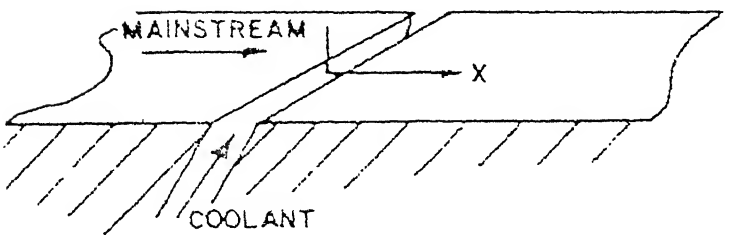

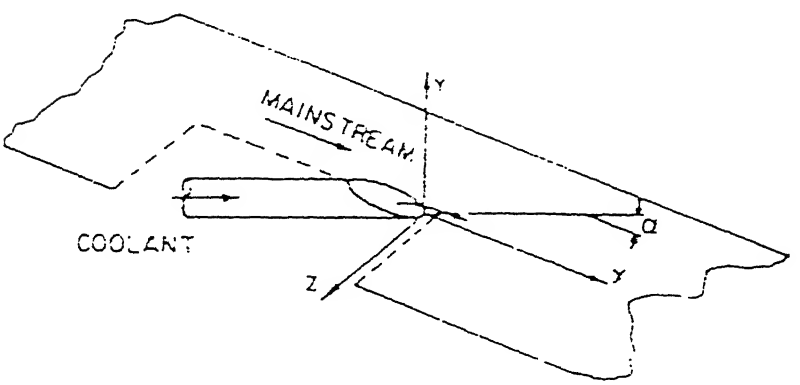

(b)

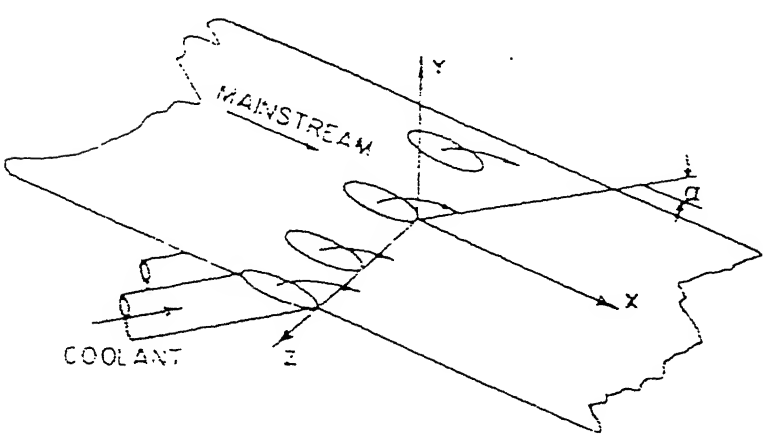

Fig 1.1 Different types of film cooling

The geometry and the flow field at the point of injection are significant variables in film cooling. The secondary fluid can enter through a continuous slot at some angle to the wall surface and the mainstream (Fig. 1(a)).

In gas turbines the air is usually drawn from the exit of the compressor. This involves some penalty in turbine efficiency. However, a considerable gain in turbine performance outweighs this loss. In the case of a rotor blade, pressure losses can be minimised by expanding the air through adjustable slots/nozzles oriented tangentially.

Although the injection geometry can influence the film cooling performance in two-dimensional study of flow, the effect is usually of second order as compared to the geometrical effects in three-dimensional film cooling. In this latter, the injection of secondary fluid is not uniform across the span. The cool air is injected at isolated locations, often through descrete holes on the surface of intest. This can lead to a situation equivalent to jets of secondary fluid being blown off the surface. For structural reasons it is usually impossible to have a truly continuous injection slot, and therefore, interrupted slots and even rows of multiple holes have been used (Fig. 1(b)).

Although film cooling has primarily been used to reduce the convective heat transfer rate from a hot gas stream to an exposed wall, it can also be used to shield a surface from thermal radiation if the radiation absorptivity of the injectant is high. This can be effectively accomplished with gas particle suspensions or a liquid coolant.

The introduction of secondary fluid into the boundary layer during the film cooling may be considered to produce an insulating layer (film) between the wall to be protected and the gas stream flowing over it. Alternatively the injected fluid can be considered as a heat sink that effectively brings down the mean temperature in the boundary layer. The introduction of the secondary fluid into the boundary layer at a

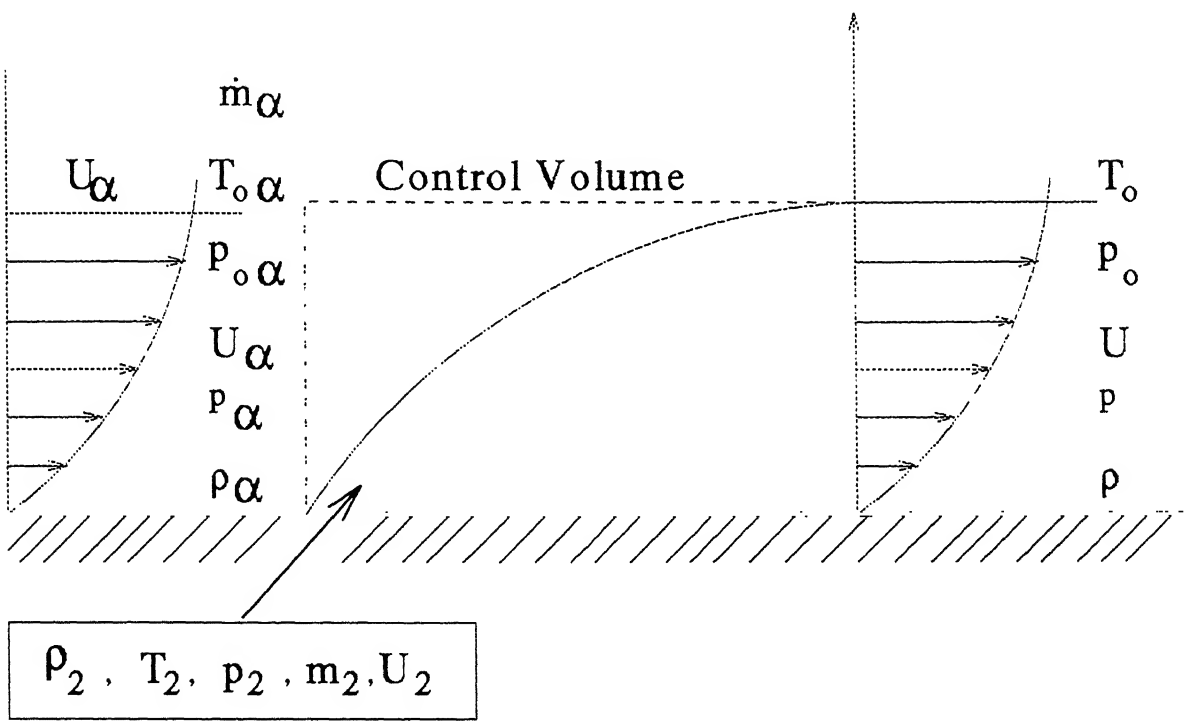
$\dot{m}_\alpha$
U_α
$T_{o\alpha}$
Control Volume
T_o
$p_{o\alpha}$
p_o
U_α
U
p_α
p
ρ_α
ρ
ρ_2 , T_2, p_2 , m_2, U_2

temperature lower than that of the mainstream and its resultant mixing with the fluid in the boundary layer reduce the temperature in the downstream. Injection of the secondary gas can increase the boundary layer thickness and the mass of the fluid entrained into the boundary layer from the free stream. The increased boundary layer thickness tends to decrease the heat transfer to the wall (Fig1.2).

The focus of the present problem is primarily on the applications, like cooling of turbine blades at the high pressure section of the turbine. It is needless to mention that the surface to be cooled in such applications is a curved one. In addition, the rotation will have an intrinsic influence on the flow field. However, for the simplicity of analysis, cooling of a flat surface has been considered in the present investigation. Eventhough the situation under consideration reveals an ideal case, the physics of jet cross flow interaction and the mechanism of coolant layer formation are well understood from such a study.

1.2 SOME BASIC DEFINITIONS

Let us consider the flow described by Fig. 1.2 The external stream static temperature is T_α, the film temperature is T_f, and the local wall temperature is T_w. The heat flux between the mainstream and the surface in presence of film cooling is given by

$$q = h\,(T_w - T_{aw})$$

where, T_{aw} is called the adiabatic wall temperature and represents the surface temperature of a perfectly insulated surface and h is the film heat transfer coefficient.

In absence of film cooling, the recovery temperature is given by

$$T_r = T_\infty \left\{ 1 + r \frac{\gamma - 1}{2} M_\infty^2 \right\}$$

$$= \frac{T_{o\infty}\left\{1 + r\frac{\gamma - 1}{2}M_\infty^2\right\}}{\left\{1 + \frac{\gamma - 1}{2}M_\infty^2\right\}}$$

In the above expression, r is known as recovery factor and expressed as

$$r = \frac{T_r - T_\infty}{U_\infty^2 / 2C_p}$$

It has been found by Eckert and Drake (1972) that $r = \sqrt{P_r}$ for laminar flows and $r = (P_r)^{1/3}$ for turbulent flows. For incompressible flows, T_r, T_∞ and $T_{o\infty}$ are nearly identical and the film cooling effectiveness may be expressed as

$$\eta = \frac{T_{aw} - T_\infty}{T_{o2} - T_\infty}$$

where, T_{o2} is the stagnation temperature of the coolant near the entry. For high speed flows ($M_\infty \geq 0.3$), the cooling effectiveness is given by

$$\eta = \frac{T_{aw} - T_r}{T_{2_r} - T_r}$$

The cooling effectiveness is basically a function of the blowing ratio ($\rho_2 U_2 / \rho_\infty U_\infty$), the density ratio ($\rho_2/\rho_\infty$), the geometry of the injection hole, the distance from the injection hole (X), and the injection angle (α).

The experimental results of film cooling have been well documented by Goldstein (1971). Jabbari and Goldstein (1978) have developed a correlation for the film cooling effectiveness from their experimental study as

$$\eta = \frac{1.9(\mathrm{Pr})^{2/3}}{1 + 0.329\left(\frac{C_{p\infty}}{C_{p2}}\right)\xi^{0.8}\beta}$$

$$\xi = \frac{X}{(\rho_2 U_2 / \rho_\infty U_\infty)L}\cdot\left[\left(\frac{\mu_2}{\mu_\infty}\right)\mathrm{Re}_2\right]^{-0.25}$$

$$\beta = 1 + 1.5 \times \mathrm{Re}^{-4} \mathrm{Re}_2 \left(\frac{\mu_2 W_\alpha}{\mu_\alpha W_2} \right) \sin \alpha$$

where W is the molecular weight, $Re_2 = \rho_2 U_2 L/\mu_2$ and L is the equivalent slot width (characteristic length of the injecting hole).

We may mention that the early developments of computational methods addressing the film cooling problem were aimed at matching the above mentioned correlation. However, a tremendous development has taken place in the areas of numerical modeling and the experimental techniques ever since the paper of Jabbari and Goldstein (1978) was published. A concise description all these studies have been documented in a subsequent chapter (Chapter 2).

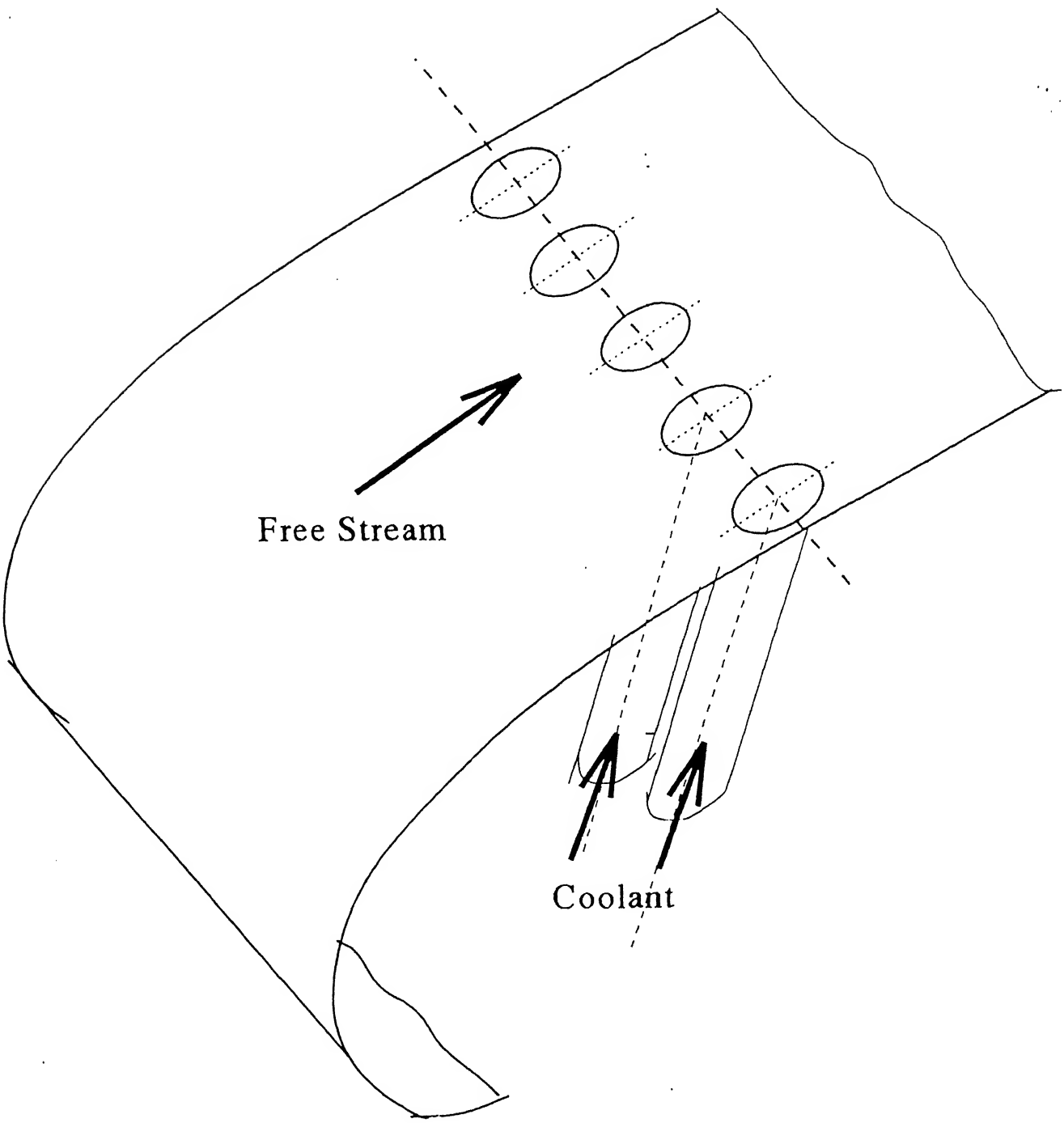

Fig 1.3 A Film cooled Turbine Blade section

1.3 SCOPE OF THE PRESENT INVESTIGATION

The importance and application of film cooling have already been enumerated in the earlier section. The pertinent parameters which govern the cooling effectiveness significantly are the blowing ratio, the angle of injection of the cooling fluid, and the velocity profile of the coolant at the exit of the injection hole. A need has been felt to analyse and understand the influence of the pertinent parameters on the effectiveness for a situation with multiple injection holes on a plate. This analysis will form a building block which can be enhanced to mimic a wide range of operating conditions encountered in practice. The aim of the present investigation is to study primarily the effect of injection velocity profile, angle of injection and blowing ratio on the film cooling effectiveness. The flow regime for such applications is usually turbulent. The analysis concerning nuances of turbulence is beyond the scope of this work. However, we have used Baldwin-Lomax (1978) model for the present computation. For the purpose of further improvement of the predictive procedure, we have embarked on a modification of the Baldwin-Lomax model. Finally an effort has been undertaken to compare the numerical results with their experimental counterpart due to Schiffer and Hennecke (1991).

Chapter 2

LITERATURE REVIEW

2.1 FILM COLLING OF FLAT PLATE GEOMETRY

A brief review of the literature pertaining to film cooling over a flat plate and a turbine blade is presented here to illustrate the state-of-the-art. The research in the field started with study of slot injection and porous injection in which adiabatic effectiveness over the plate could be obtained by using a two dimensional model of the flow field. The study on the flow field due to injection through a single hole and a row of holes followed these investigations, The evaluation of complex flow fields necessitated a three dimensional analysis. Subsequent investigations, in this field include the influence of different parameters such as the blowing ratio, density ratio, length to diameter ratio of inlet pipe, the free stream and jet turbulence, the state of the incoming boundary layer and so on. An excellent review by Goldstein (1971) describes some of these factors and earlier experimental investigations on film cooling.

The fundamental research on film cooling started since 1950. But the first research report was published from the University of Minnesota by Goldstein et al. (1968). They considered injection through a single circular hole for their study. This was followed by a report of Goldstein et al. (1970) which addresed the issues concerning the injection through a series of holes.

Till 1970, the study was carried out with density ratios around 1.0 and very low blowing ratios. In one of the earlier computational works (Launder et al. (1978)) a three dimensional analysis of a turbulent jet from a circular hole in a cross flow was accomplished. They considered a low blowing ratio.

Foster et al. (1980), have conducted experimental study on the flow and film cooling effectiveness for the case of injection through a row of holes. The experimental results include the influence of various injection angles, at different hole spacings and blowing rates. They reported that at small injection angles the effectiveness is high for low blowing ratios. On the other hand at high injection angles the effectiveness is high for high blowing ratios. Closer hole spacings improved the lateral coverage and alleviate jet lift-off effects.

Demuren et al. (1986) reported a systematic study of film cooling with a three dimensional calculation procedure. They presented the effect of different parameters on the cooling effectiveness for one row of holes. They used standard k-ε model for evaluating turbulent stresses and heat fluxes. They deployed the locally - elliptic procedure of Rodi and Srivatsa (1980), which allows the full elliptic treatment to a small region containing reverse flow. However, in the near and the far fields, the model reverts to the partially parabolic and fully-parabolic schemes respectively.

Although Foster and Lampard (1980), Firth and Jones (1988) have covered a wide range of density and blowing ratios, one feature they had in common was the use of large length-to-diameter ratio of the entry port. Such a configuration is not representative of a gas turbine. Sinha et al. (1991) have conducted experiments using length-to-diameter ratio of 1.75. They have also calculated adiabatic film cooling effectiveness for a large number of density and blowing ratios for a row of 35°

inclined holes with pitch-to-diameter ratio of 3. Schiffer and Hennecke (1991) experimentally studied the influence of gas temperature on the film cooling effectiveness. The temperature of the hot gas was varied between 420 K and 780 K. The free stream Mach number was 0.4. The experiments were performed on a flat plate with a row of inclined holes at an angle of 30° and pitch-to-diameter ratio of 2. As per the author`s knowledge, this is perhapes investigation, cited in open literature where the test facility used hot gas to estimate film cooling effectiveness over a flat plate. Thus the flow environment in the above mentioned experiment closely represents the mechanism of film cooling in a gas turbine.

Amer et al. (1992) presented a comparison of different two-equation turbulence models for prediction of film cooling effectiveness for two rows of holes. The models used include k-ω model, a modified k-ω model, that k-ε model together with a modification of anisotropic turbulence. The analysis reveals that the prediction of effectiveness depends on the blowing ratio and the distance downstream of the injection hole. They used the PHONICS code to solve the governing equations. The study indicates that the two-equation turbulence models do not work well for the film cooling problem especially in the vicinity of the holes.

Leylek and Zerkle (1994) have conducted a large scale computational analysis and compared their results with earlier experimental results of Sinha et al. (1991). The three dimensional Naveir Stoke equations have been solved to analyse the jet-crossflow interaction. Their analysis compares favourably with the experimentally observed, velocity profiles (due to Pietrzyle et al., 1989) at the exit port due to interaction with main stream for different blowing ratios.

In the case of low length to diameter (L/D) ratio and for blowing ratio of approximately 0.5, the exit velocity profile is almost similar to a fully developed turbulent profile (1/7th low profile). For blowing ratios above 0.5, the velocity profile is skewed with the peak shifted towards the upstream direction. Similarly for blowing ratios below 0.5, the peak is shifted towards the downstream. Near the hole, the effectiveness is not well predicted. Moreover, the lateral spreading of the coolant is underpredicted due to an isotropic nature of the flow field near the injection region.

The aerodynamics of a coolant jet in an environment, which is representative of what prevails in a gas turbine has been numerically investigated for film cooling applications by Sarkar and Bose (1995). The time dependent mass averaged NS equations coupled with the compressible form of a two equation low Reynolds number k-ε model have been solved using an explicit finite volume formulation. The results present the effect of blowing rates, slot angle, and the free stream turbulence at the inlet. They have also analysed the performance of five different turbulence models in predicting the flow-field and heat transfer phenomena created by the jet-crossflow interactions pertaining to film cooling.

Sarkar and Bose (1997) have presented another numerical study of film cooling with three dimensional calculation for injection through descrete holes on a flat plate. The results presented illustrate the variation of complex aerodynamics and heat transfer phenomena in a jet cross flow interaction. The simulation comprises solving the three dimensional and Navier Stokes Equations (mass averaged) along with the algebraic turbulence model of Baldwin and Lomax (1978).

2.2 ADVANCED RESEARCH IN FILM COOLING

Although the present work is restricted to the numerical simulation of discrete jet film cooling over a flat plate, some recent work of film cooling over turbine blade are sited below:

Sarkar and Bose (1995) demonstrated the aero-thermal behaviour of coolant jet over the VKI turbine blade for different blowing ratios and angles of injection. A three-dimensional simulation by Sarkar (1997) also indicates the mechanism of coolant layer formation over a highly curved vane and a layer of contra-rotating parallel vertices. This study illustrates that the formation of coolant layer on the pressure surface is critical and the regions between two adjacent holes are not well protected.

Garg et al. (1997) investigated the effect of velocity and temperature distribution at the exit of the hole on film cooling of turbine blades. Garg and Abhari (1997) simulated film cooling on a transonic rotating rotor blade and compare their results with the experimental observation. On the pressure side, the experimental result is under predicted. The turbulence is simulated by the Baldwin-Lomax model. The authors prefer to use the Baldwin-Lomax model considering the fact that, it is simple and relatively economical compared to two equation models. They also indicate that the two equation models are not found suitable for film cooling applications.

Chapter 3

STATEMENT OF THE PROBLEM

3.1 OBJECTIVES OF THE PRESENT WORK

The main objectives of the present work are to simulate the complex jet cross flow interaction in film cooling applied to a flat plate with injection of secondary fluid through a series of circular holes and study the effect of different parameters on the effectiveness of film cooling. The parameters considered here for study include the blowing ratio, the angle of injection and the velocity profile of the secondary fluid at the exit of the blowing hole.

The Reynolds averaged (Farve averaged) three dimensional Navier Stokes equations and the energy equation are solved using a finite volume approach. For the modeling of the turbulent flow, Baldwin-Lomax algebraic model has been used. The Baldwin-Lomax model has been modified in order to invoke the effects of turbulence near the injection hole. Explicit MacCormack method is deployed for solving the governing equations.

As mentioned in the literature review. Schiffer and Hennecke (1991) have accomplished film cooling experiments with hot gas as the mainstream over a flat plate. Their results for the cases of some specific governing input parametershave been considered as the basis of comparison of our predictive procedure. Leylek and Zerkle (1994) have indicated about various exit velocity profiles at the injection holes

for different physical situations. These profiles include the fully developed turbulent pipe flow and the skewed velocity profiles. We have considered all these possible cases in our study including a uniform profile at the exit of the hole. The results obtained have been discussed in a subsequent chapter.

3.2 GOVERNING EQUATIONS

The Reynolds averaged Navier-Stokes Equations of fluid motion and energy equation can be non dimensionalised using the flowing non-dimensional variables.

$$x^* = \frac{x}{D},\ y^* = \frac{y}{D},\ z^* = \frac{z}{D}$$

$$u^* = \frac{\bar{u}}{U_\alpha},\ v^* = \frac{\bar{v}}{U_\alpha},\ w^* = \frac{\bar{w}}{U_\alpha}$$

$$\rho^* = \frac{\rho}{\rho_\alpha},\ T^* = \frac{\bar{T}}{T_\alpha},\ t^* = \frac{tU_\alpha}{D}$$

$$p^* = \frac{\bar{p}}{\rho_\alpha U_\alpha^2},\ e^* = \frac{\bar{e}_t}{U_\alpha^2}$$

All the barred quantities in the above equlities are Favre averaged (1965) quantities for a turbulent flow. On the basis of the nondimensional procedure mentioned above, the Reynolds number and the prandtl number are defined as

$$\mathrm{Re}_\alpha = \frac{\rho_\alpha U_\alpha D}{\mu_\alpha}$$

$$\mathrm{Pr} = \frac{\mu cp}{k}$$

The coefficient of viscosity (μ) is a function of temperature of the gas and is calculated by the Sutherland's equation in the following way:

$$\mu = 1.456 \times 10^{-6}\left[\frac{T^{3/2}}{T + 101.4}\right]$$

The equations of fluid motion and energy after nondimensionalisation can be written as:

1. **Continuity Equation**

$$\frac{\partial \rho^*}{\partial t^*} + \frac{\partial}{\partial x^*}\left(\rho^* u^*\right) + \frac{\partial}{\partial y^*}\left(\rho^* v^*\right) + \frac{\partial}{\partial z^*}\left(\rho^* w^*\right) = 0 \tag{3.1}$$

2. **X-Component of Momentum Equation**

$$\frac{\partial}{\partial t^*}\left(\rho^* u^*\right) + \frac{\partial}{\partial x^*}\left(\rho^* u^{*2} + p^*\right) + \frac{\partial}{\partial y^*}\left(\rho^* u^* v^*\right) + \frac{\partial}{\partial z^*}\left(\rho^* u^* w^*\right) = \frac{\partial}{\partial x^*}\left(\tau_{xx}^*\right) + \frac{\partial}{\partial y^*}\left(\tau_{xy}^*\right) + \frac{\partial}{\partial z^*}\left(\tau_{xz}^*\right) \tag{3.2}$$

3. **Y-Component of Momentum Equation**

$$\frac{\partial}{\partial t^*}\left(\rho^* v^*\right) + \frac{\partial}{\partial x^*}\left(\rho^* u^* v^*\right) + \frac{\partial}{\partial y^*}\left(\rho^* v^{*2} + p^*\right) + \frac{\partial}{\partial z^*}\left(\rho^* v^* w^*\right) = \frac{\partial}{\partial x^*}\left(\tau_{xy}^*\right) + \frac{\partial}{\partial y^*}\left(\tau_{yy}^*\right) + \frac{\partial}{\partial z^*}\left(\tau_{yz}^*\right) \tag{3.3}$$

4. **Z-Component of Momentum Equation**

$$\frac{\partial}{\partial t^*}\left(\rho^* w^*\right) + \frac{\partial}{\partial x^*}\left(\rho^* u^* w^*\right) + \frac{\partial}{\partial y^*}\left(\rho^* v^* w^*\right) + \frac{\partial}{\partial z^*}\left(\rho^* w^{*2} + p^*\right) = \frac{\partial}{\partial x^*}\left(\tau_{xz}^*\right) + \frac{\partial}{\partial y^*}\left(\tau_{yz}^*\right) + \frac{\partial}{\partial z^*}\left(\tau_{zz}^*\right) \tag{3.4}$$

5. **Energy Equation**

$$\frac{\partial}{\partial t^*}\left(\rho^* e^*\right) + \frac{\partial}{\partial x^*}\left(\rho^* u^* e^* + p^* u^*\right) + \frac{\partial}{\partial y^*}\left(\rho^* v^* e^* + p^* v^*\right) + \frac{\partial}{\partial z^*}\left(\rho^* w^* e^* + p^* w^*\right)$$
$$= \frac{\partial}{\partial x^*}\left(u^* \tau_{xx}^* + v^* \tau_{xy}^* + w^* \tau_{xz}^* - q_x^*\right) + \frac{\partial}{\partial y^*}\left(u^* \tau_{yx}^* + v^* \tau_{yy}^* + w^* \tau_{yz}^* - q_y^*\right) \tag{3.5}$$
$$+ \frac{\partial}{\partial z^*}\left(u^* \tau_{zx}^* + v^* \tau_{zy}^* + w^* \tau_{zz}^* - q_z^*\right)$$

where,

$$\tau_{xx}^* = \frac{\mu^* + \mu_t^*}{\mathrm{Re}_a}\left[2\frac{\partial u^*}{\partial x^*} - \frac{2}{3}\left(\nabla^* . \vec{V}^*\right)\right]$$

$$\tau^*_{xy} = \tau^*_{yx} = \frac{\mu^* + \mu^*_t}{\mathrm{Re}_\alpha}\left[\frac{\partial u^*}{\partial x^*} + \frac{\partial v^*}{\partial y^*}\right]$$

$$\tau^*_{xz} = \tau^*_{zx} = \frac{\mu^* + \mu^*_t}{\mathrm{Re}_\alpha}\left[\frac{\partial w^*}{\partial x^*} + \frac{\partial u^*}{\partial z^*}\right]$$

$$\tau^*_{yy} = \frac{\mu^* + \mu^*_t}{\mathrm{Re}_\alpha}\left[2\frac{\partial v^*}{\partial y^*} - \frac{2}{3}\left(\nabla^*.\vec{V}^*\right)\right]$$

$$\tau^*_{zy} = \tau^*_{yz} = \frac{\mu^* + \mu^*_t}{\mathrm{Re}_\alpha}\left[\frac{\partial v^*}{\partial z^*} + \frac{\partial w^*}{\partial y^*}\right]$$

$$\tau^*_{zz} = \frac{\mu^* + \mu^*_t}{\mathrm{Re}_\alpha}\left[2\frac{\partial w^*}{\partial z^*} - \frac{2}{3}\left(\nabla^*.\vec{V}^*\right)\right]$$

$$q_x = -\frac{1}{\mathrm{Re}_\alpha(\gamma-1)M^2_\infty}\left[\frac{\mu^*}{\mathrm{Pr}} + \frac{\mu^*_t}{\mathrm{Pr}_t}\right]\frac{\partial T^*}{\partial x^*}$$

$$q_y = -\frac{1}{\mathrm{Re}_\alpha(\gamma-1)M^2_\infty}\left[\frac{\mu^*}{\mathrm{Pr}} + \frac{\mu^*_t}{\mathrm{Pr}_t}\right]\frac{\partial T^*}{\partial y^*}$$

$$q_z = -\frac{1}{\mathrm{Re}_\alpha(\gamma-1)M^2_\infty}\left[\frac{\mu^*}{\mathrm{Pr}} + \frac{\mu^*_t}{\mathrm{Pr}_t}\right]\frac{\partial T^*}{z^*}$$

In the above equations, Pr is the Prandtl number of the fluid which has ben taken as 0.7 and Pr_t is the turbulent Prandtl number. A value of 0.9 has been used as turbulent Prandtl number.

The above set of Favre averaged Navier-Stokes equations and the energy equation can be written in the following strong conservative form. The prefix '*' is omitted at this stage for convenience. However, all the variables are necessarily non-dimensional.

$$\frac{\partial U}{\partial t} + \frac{\partial E}{\partial x} + \frac{\partial F}{\partial y} + \frac{\partial G}{\partial z} = H \qquad (3.6)$$

where

$$U = \begin{Bmatrix} \rho \\ \rho u \\ \rho v \\ \rho w \\ \rho e \end{Bmatrix}$$

$$E = \begin{bmatrix} \rho u \\ \rho u^2 + p - \tau_{xx} \\ \rho uv - \tau_{xy} \\ \rho uw - \tau_{yz} \\ (\rho e + p - \tau_{xx})u - \tau_{xz}w - \tau_{yx}v - q_x \end{bmatrix}$$

$$F = \begin{bmatrix} \rho v \\ \rho uv - \tau_{xy} \\ \rho v^2 + p - \tau_{yy} \\ \rho vw - \tau_{yz} \\ \left(\rho e_t + p - \tau_{yy}\right)v - \tau_{yx}u - \tau_{yz}w + q_y \end{bmatrix}$$

$$G = \begin{bmatrix} \rho w \\ \rho uw - \tau_{xz} \\ \rho vw - \tau_{yz} \\ \rho w^2 + p - \tau_{zz} \\ (\rho e + p - \tau_{zz})w - \tau_{xz}u - \tau_{yz}v - q_z \end{bmatrix} \qquad H = \begin{bmatrix} 0 \\ 0 \\ 0 \\ 0 \\ 0 \end{bmatrix}$$

3.3 TURBULENCE MODEL

The quantity, μ_t in the earlier equations is the eddy viscosity or the turbulent viscosity and it is calculated using an algebraic model called Baldwin-Lomax model (1978). The Baldwin-Lomax model is described herein.

3.3.1 Baldwin-Lomax Model

Baldwin-Lomax (1978) model is a two layer algebraic eddy viscosity model in which μ_t is given by

$$\mu_t = \begin{cases} \mu_{t_{inner}} & y \le \delta \\ \mu_{t_{outer}} & y > \delta \end{cases}$$

where, δ is the smallest normal distance from wall at which the inner and the outer formulae are equal.

For the inner region, Prandtl-Van Driest formulation is used which is given by

$$\mu_{t_{inner}} = \rho l^2 |w| \tag{3.7}$$

where

$$l = \kappa y\left[1 - \exp\left(-y^+ / A_0^+\right)\right]$$

and

$|w|$ is the magnitude of $\vec{w}$ (vorticity) given by

$$|w| = \left[\left(\frac{\partial V}{\partial x} - \frac{\partial U}{\partial y}\right)^2 + \left(\frac{\partial W}{\partial y} - \frac{\partial V}{\partial z}\right)^2 + \left(\frac{\partial U}{\partial z} - \frac{\partial W}{\partial x}\right)^2\right]^{1/2}$$

and

$$y^+ = \frac{\rho_w U_\tau y}{\mu_w} = \frac{\sqrt{\rho_w \tau_w}}{\mu_w}.y$$

For the outer region (From Closure Formulation)

$$(\mu_t)_{outer} = kC_{cp}\rho F_{wake} F_{kLeb}(y) \tag{3.8}$$

where k is the closure constant ≈ 0.41

C_{cp} is an additional constant ≈ 1.6

$$F_{wake} = \min\begin{Bmatrix} Y_{\max} F_{\max} \\ C_{wk} Y_{\max} u_{dif}^2 / F_{\max} \end{Bmatrix}$$

The quantities F_{max} and Y_{max} are determined from the function

$$F(y) = y|w|\left[1 - \exp(-y^+ / A^+)\right]$$

The Klebanoff intermittency factor,

$$F_{kleb}(y) = \left[1 + 5.5\left(\frac{C_{Kleb}y}{Y_{\max}}\right)^6\right]^{-1}$$

U_{dif} is the difference between maximum and minimum total velocity in the profile.

$$U_{dif} = \sqrt{\left(U^2 + V^2 + W^2\right)_{\max}} - \sqrt{\left(U^2 + V^2 + W^2\right)_{\min}}$$

In effect, the distribution of vorticity is used to determine length scaler so that the necessity for finding the outer edge of the BL is removed.

3.3.2 Modification Of Baldwin-Lomax Model (Relaxation Model)

A relaxation model is generally used to account for the complicated interaction of scaling in spatial response to the turbulent structure in a rapidly changing flow field such as flow over a rearward or a forward facing step.

When a secondary coolant is injected into the hot cross flow, there occurs a blockage effect with local acceleration of the crossflow over the coolant jet and a wake region is evolved with flow reversals. Thus in the present environment, it has been decided to incorporate the relaxation technique of Waskiewicz et al in an attempt to account for the upstream turbulence history effect.

The relaxation eddy viscosity is given by

$$\mu_t = \mu_{eq} + \left(\mu_{ups} - \mu_{eq}\right)\exp\left[\frac{-(x - x_o)}{\lambda\delta_o}\right] \qquad \text{for } x \geq x_o \qquad (3.9)$$

where, μ_{eq} is the calculated equilibrium value of eddy viscosity obtained from the Baldwin-Lomax model and μ_{ups} denotes the value of the eddy viscosity at a location (x_o) upstream of the injection. At this location the surface pressure rise begins owing to the injected fluid. The quantity δ_o is the boundary layer thickness at x_o. The parameter λ is the relaxation length scale which represents the lag-response of the

turbulent stress to the sudden change of the flow gradient. The condition $\lambda = \alpha$ implies that the eddy viscosity at all streamwise locations downstream of the interaction is frozen to initial upstream values (μ_{ups}). It is assumed that $\lambda = 7.5$ will characterise the present turbulent mixing.

Chapter 4

NUMERICAL METHOD

4.1 FINITE VOLUME FORM OF GOVERNING EQUATIONS

The unsteady three dimensional mass averaged Navier-Stokes Equations described in the previous chapter are marched in time using explicit, second order accurate timesplit, cell centred finite volume scheme based on MacCormack [1972] until the steady state is reached.

Rewriting the equation (3.6)

$$\frac{\partial U}{\partial t}+\frac{\partial E}{\partial x}+\frac{\partial F}{\partial y}+\frac{\partial G}{\partial z}=H$$

Integration of the above equation over a finite volume leads to its integral form as,

$$\frac{\partial}{\partial t}\int_{\Omega} U d\Omega+\int_{s}\overline{Q}.\overline{ds}=\int_{\Omega} H d\Omega=0 \qquad \text{(As H = 0)}$$

$$\frac{\partial U}{\partial t}+\frac{1}{\Omega_{ijk}}\int_{s}\overline{Q}.\overline{ds}=0 \qquad (4.1)$$

where

Ω_{ijk} denotes the volume of the cell (i,j,k)

$\overline{ds}$ denotes the surface normal vector

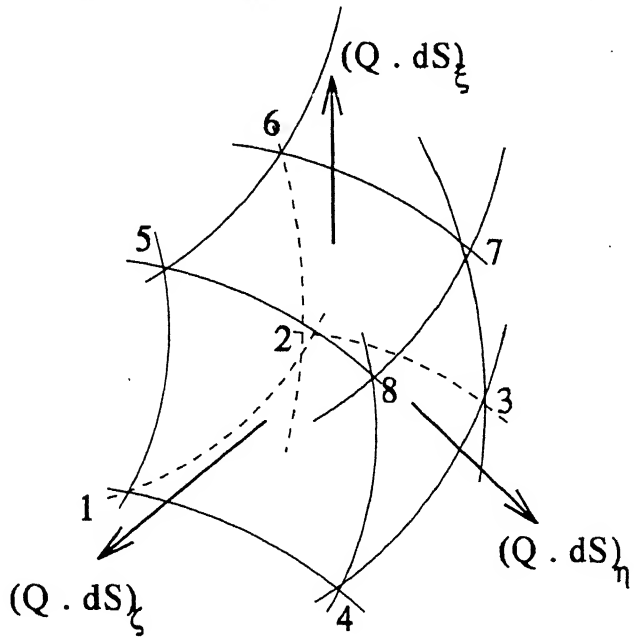

A Finite volume in non-orthogonal coordinates

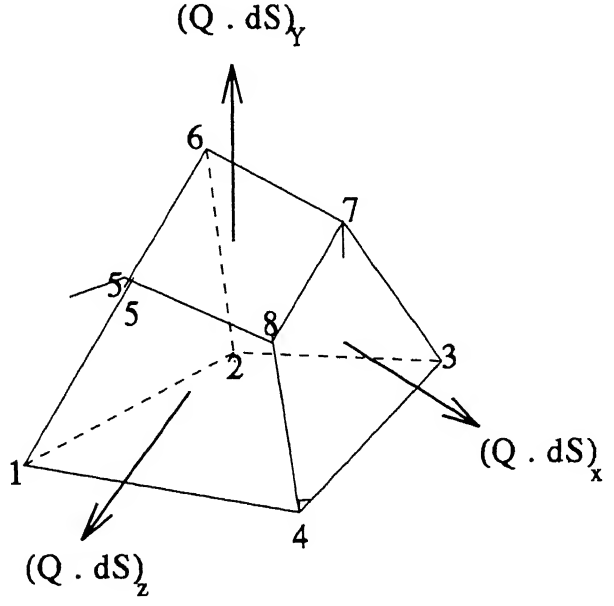

A Finite volume in orthogonal coordinates

Fig. 4.1

$\overline{Q}$ is the flux vector of E, F and G

These systems of equations can be solved in the x, y, z coordinate system for a control volume shown in Fig. 4.1 by application of the Explicit MacCormack algorithm.

4.2 EXPLICIT MACCARMACK METHOD

The unsteady equations are solved by LI, LJ, and LK operators as explained by MacCarmack (1972). In each of the operator the solution proceeds in one of the three coordinate systems, x, y and z. Each operator has the predictor and the corrector steps. In the predictor step, the fluxes are calculated using the variables at known time level. In the corrector step, the predicted value is corrected to get the value of the variable at the present time level. In the predictor step the flux $\overline{Q}.ds$ is evaluated by backward differencing whereas in the corrector step it is evaluated by forward differencing. This procedure is repeated till steady state solution is reached.

LI (Δt) Operator

Predictor

$$\tilde{U}^{*}_{ij} = U^{\eta}_{ij} - \frac{\Delta t}{\Omega_{ij}}\left[Q^{\eta}_{ij}.\overline{S}_{i+1} + \overline{Q}^{\eta}_{i-1}.\overline{S}_{i}\right]$$

Corrector

$$\tilde{U}^{*}_{ij} = \frac{1}{2}\left[U^{\eta}_{ij} + \tilde{U}^{*}_{ij} - \frac{\Delta t}{\Omega_{ij}}\left(Q^{*}_{i+1}.S_{i+1} + Q^{*}_{ij}.\overline{S}_{i}\right)\right]$$

For stability

$$\Delta t_x \le \min\left\{\frac{\Omega_{ij}}{\left|\overline{q}.\overline{S}_i\right| + c\left|S_i\right| + \frac{1}{\rho}\left(\mu + \frac{2r\mu}{\Pr}\right)\left\{\left(\left|\overline{S}_i\right|^2 + \left|\overline{S}_i\right|\left|\overline{S}_j\right| + \left|S_i\right|\left|S_k\right|\right)/\Omega_{ijk}\right\}}\right\}$$

where c = $\sqrt{\gamma RT}$

LJ (Δt) Operator

Predictor

$$\tilde{U}_{ij}^{*} = U_{ij}^{\eta} - \frac{\Delta t}{\Omega_{ij}}\left[Q_{ij}^{\eta}.\bar{S}_{j+1} + \bar{Q}_{ij-1}^{\eta}.\bar{S}_{j}\right]$$

Corrector

$$\tilde{U}_{ij} = \frac{1}{2}\left[U^{\eta} + \tilde{U}_{ij}^{*} - \frac{\Delta t}{\Omega_{ijk}}\left(\tilde{Q}_{i+1}^{*}.\bar{S}_{j+1} + Q^{*}.\bar{S}_{j}\right)\right]$$

For stability

$$\Delta t_{y} \leq \min\left\{\frac{\Omega_{ijk}}{\left|\bar{q}.\bar{S}_{j}\right| + c\left|S_{j}\right| + \frac{1}{\rho}\left(\mu + \frac{2r\mu}{\Pr}\right)\left\{\left(\left|\bar{S}_{j}\right|^{2} + \left|\bar{S}_{j}\right|\left|\bar{S}_{i}\right| + \left|S_{j}\right|\left|S_{k}\right|\right)/\Omega_{ijk}\right\}}\right\}$$

where c = $\sqrt{\gamma RT}$

LK (Δt) Operator

Predictor

$$\tilde{U}_{ijk}^{*} = U_{ijk}^{\eta} - \frac{\Delta t}{\Omega_{ijk}}\left[Q_{k}^{\eta}.\bar{S}_{k+1} + \bar{Q}_{k-1}^{\eta}.\bar{S}_{k}\right]$$

Corrector

$$\tilde{U}^{\bullet}_{ijk} = \frac{1}{2}\left[U^{\eta}_{ijk} + \tilde{U}^{\bullet}_{ijk} - \frac{\Delta t}{\Omega_{ijk}}\left(Q^{\bullet}_{k+1}.S_{k+1} + Q^{\bullet}_{k}.\bar{S}_{k} \right) \right]$$

For stability

$$\Delta t_{\zeta} \leq \min\left\{ \frac{\Omega_{ikj}}{\left|\bar{q}.\bar{S}_k\right| + c\left|S_k\right| + \frac{1}{\rho}\left(\mu + \frac{2r\mu}{\Pr}\right)\left\{\left(\left|\bar{S}_k\right|^2 + \left|\bar{S}_k\right|\left|\bar{S}_i\right| + \left|S_k\right|\left|S_j\right|\right)/\Omega_{ijk}\right\}} \right\}$$

where $c = \sqrt{\gamma RT}$

Using the above operators, the U^{n+1}_{ijk} is obtained by operating the LI, LJ, and LK operators in the following sequence.

$$U^{n+1}_{ijk} = \left[LJ(\Delta t/2)LK(\Delta t/2)LI(\Delta t)LK(\Delta t/2)LJ(\Delta t/2) \right] U^{n}_{ijk}$$

where,

$$\Delta t = \min\{\Delta t_x, 2\,\Delta t_y, 2\Delta t_z\}$$

The surface vector (Fig. 4.1) used above is written in mathematical form as

$$S_{1234} = \frac{1}{2}\left(\vec{r}_{24} \times \vec{r}_{13}\right)$$

$\vec{r}_{13}, \vec{r}_{24}$ unit vector of the diagonals.

The volume of the cell ijk (Fig. 4.1) is calculated mathematically as,

$$\Omega = \frac{1}{3}\vec{r}_{17}\left[\bar{S}_{1234} + \bar{S}_{1265} + \bar{S}_{1485}\right]$$

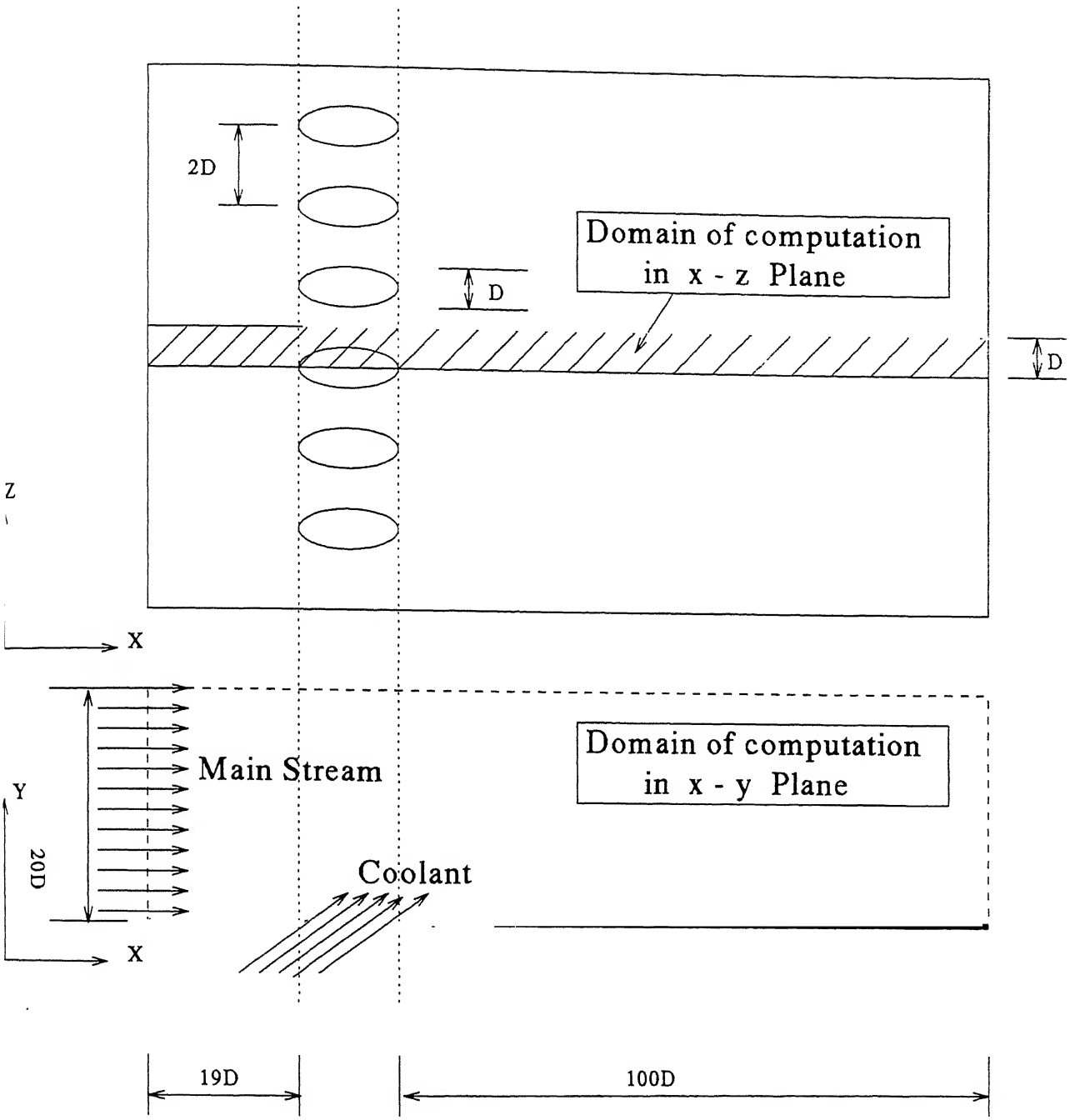

Fig. 4.2 Computational Domain

4.3 COMPUTATIONAL DOMAIN

4.3.1 Grid Generation

The geometry consists of a flat plate with desecrate holes of diameter, D = 4mm. An algebraically generated non-uniform Cartesian mesh consisting of 85x40x20 grid points is used as the computational domain. The pitch to diameter ratio is taken as 2. Because of the use of rectangular grids, the edge of the exit hole has to be approximated by steps. Due to limited computational facilities, the grid size is restricted to the configuration mentioned above. The grid is generated by placing a number of fine uniform grid points within the hole region and stretching the grid in all the three directions. A fine exponentially stretched mesh spacing is employed in the near hole region, and a course uniform grid is used far away from the hole of injection.

4.3.2 Boundary Conditions

Boundary conditions are specified at all the six boundaries of the computational domain under study. At the inflow boundary, the total pressure and total temperature are specified. The static pressure is extrapolated from the interior and hence the other variables at the inlet are updated for each time integration. The exit plane is positioned far downstream of the injection (100 D) so that a Neumann condition can be applied for all variables at this plane. On the solid surface, i.e. on the plate face, no slip conditions are imposed alongwith normal temperature gradient as zero to satisfy the adiabatic wall condition. The upper boundary of the computational domain is chosen sufficiently far from the plate and a 'slip-wall' type boundary condition is applied at this plane of boundary. The flow is symmetric with respect to x-y plane through both the centre of the injection hole and midway between the two adjacent holes. A symmetric condition is

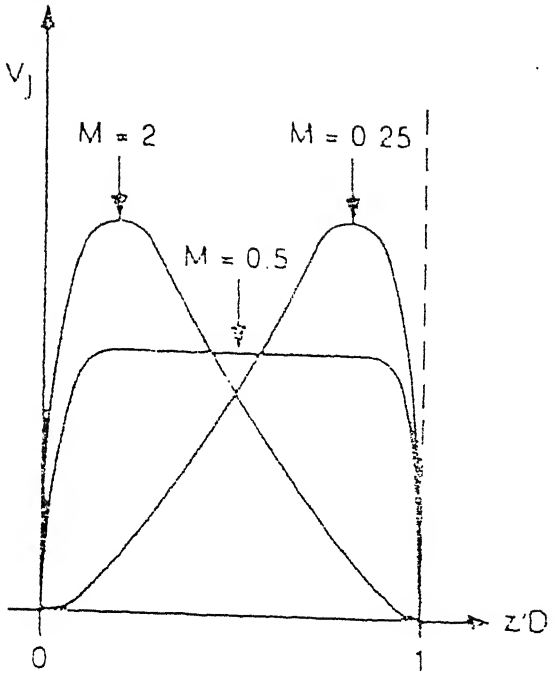

(b) Low L/D

Fig 4.3 Different hole exit velocity profiles

imposed at these boundaries by prescribing z-component of velocity vector and setting gradients of all other dependent variables in z-direction equal to zero.

4.3.3 Injection Conditions

The injection condition within the hole is difficult to specify. As a part of the present study, different velocity profiles are used for the injection condition. Leleyk and Zerkle (1994), and Pietryzk et al. (1989) have investigated computationally as well as experimentally that the injection velocity profile will be same as fully developed turbulent pipe flow in the case of a blowing ratio of 0.5. For the other cases the peak of the profile will be skewed from the axis of symmetry. Pietryzk et al. (1989) have mentioned that a uniform velocity profile will predict almost similar result to that of 1/7 th power law. In the present work all the above possible velocity profiles are used as injection condition and the effect is observed.

Chapter 5

RESULTS AND DISCUSSION

5.1 GENERAL

In most of the film cooling applications discrete holes are used for introducing the coolant. The individual jets emerging form desecrate holes in a row interact with the cross flow and thereby create a strong three dimensional flow near the injection region. The jet trajectory is bent by the interaction with the main stream and this bending produces a pair of counter rotating vortices inside the jet which modify the jet cross sectional shape to a kidney like form. The individual jet interacts with the neighbouring jets and the main stream. This interaction creates a layer of counter rotating parallel vortices which develop into the cooling film downstream of injection The flow topology corresponding to the hole injection is shown in Fig. 5.1.

For the present work, the experimental investigation of Schiffier and Hennecke (1991) is numerically simulated using the compressible Navier-Stokes equations with the Baldwin Lomax model. The relaxation technique is also incorporated into the Baldwin Lomax Model to take into the account of the upstream effect. The flow configuration and computational domain are shown in Fig. 5.2.

The boundary conditions have to be prescribed at all the confining boundaries of the computational domain which have already been discussed. However the

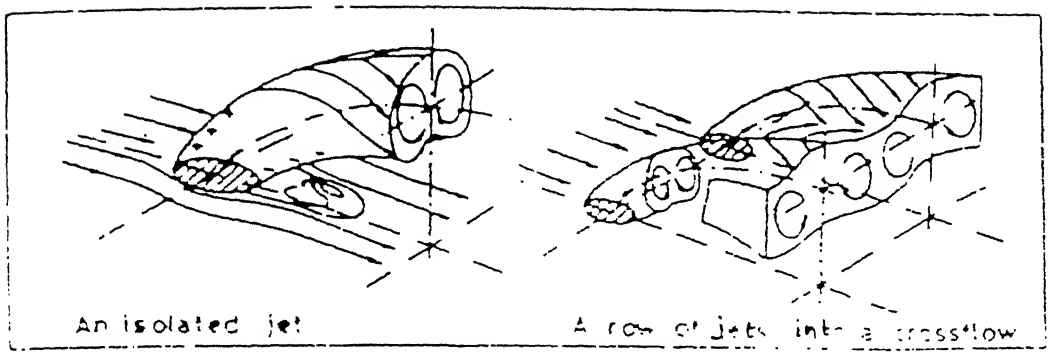

Fig 5.1 Flow field for injection through a row of holes

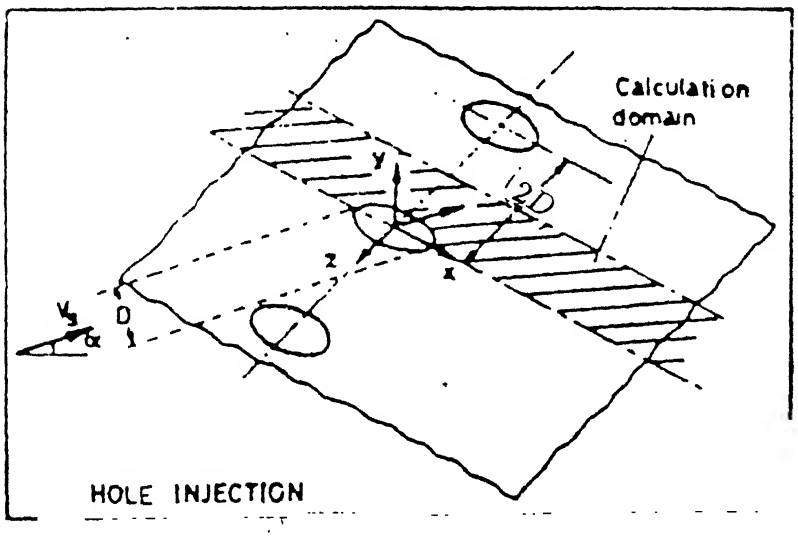

Fig 5.2 Flow configuration for injection through a row of holes

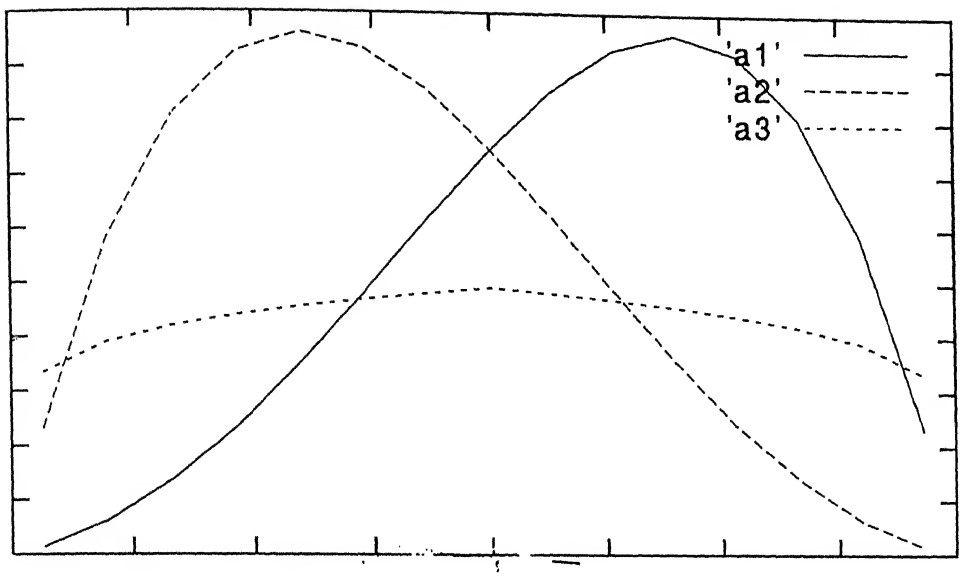

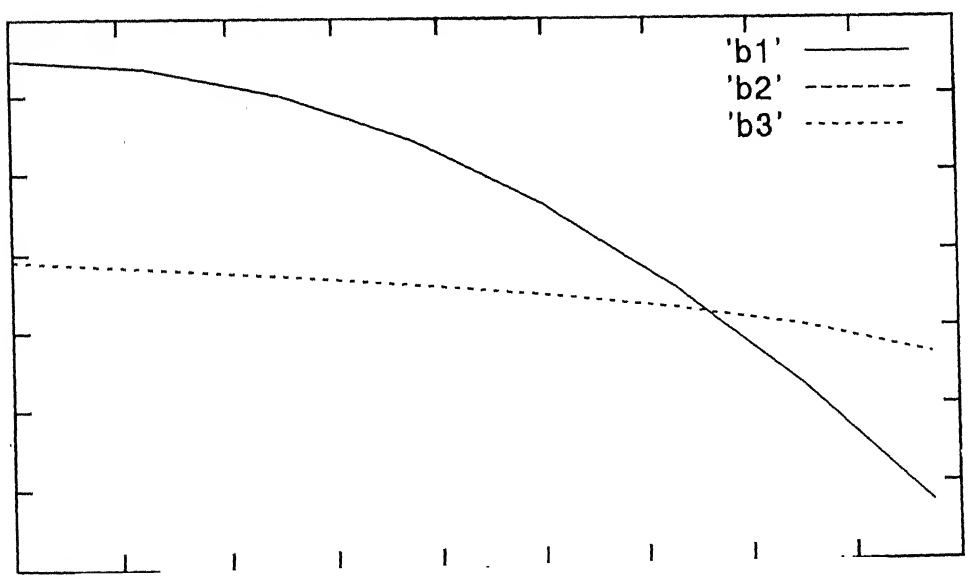

$a1, b1$: $PolynomialProfile with + ve Shift$

$a2, b2$: $PolynomialProfile with - ve Shift$

$a3, b3$: $1/7th Power Law Profile$

Fig 5.6 Computed velocity profile near the hole

specification of the flow condition at the exit of the jet is known to be a critical issue. A viable approach is to include the whole part into computational domain [Zerkle and Leylek,1994]. Experimental investigation indicates that for a low L/D ratio, which is closer to the gas turbine film cooling applications, a fully developed profile is evolved at a blowing ratio of about 0.5. At a higher blowing ratio, the jet exit profiles are skewed with a peak shifted to the upstream side whereas for a low blowing ratio the peak is shifted towards the downstream (Fig. 5.3). It has been decided to examine the effect of exit velocity profiles on the film cooling, with a low L/D ratio. The experiment of Schiffer and Hennecke (1991) has been taken up as the basis of comparison in the present invetigation. The L/D ratio used is 3.0 and the flow environment is similar to what is found in gas turbine applications. The free stream Mach number is 0.4, free stream temperature is 658 K, and Re_{α} based on the hole diameter is $2.5x10^{6}$.

All computations have been performed on a DEC Alphastation - 2000. The solution is assumed to be converged, when the value of residual have dropped by atleast 4 orders of magnitude. The steady state solution achieved in about 10000 iterations with the Baldwin Lomax models. The present computations are carried out with a 85X40X20 grid with pitch to diameter ratio of 2.0. Figure 5.4 shows the grid on x-y plane. The grid is stretched near the wall and near the injection region to capture steep gradients of flow variables. The first grid point above the wall is so chosen that the magnitude of y^{+} remains below 5.0. Because of the rectangular grid used, the edge of the exit hole has been approximated by steps.

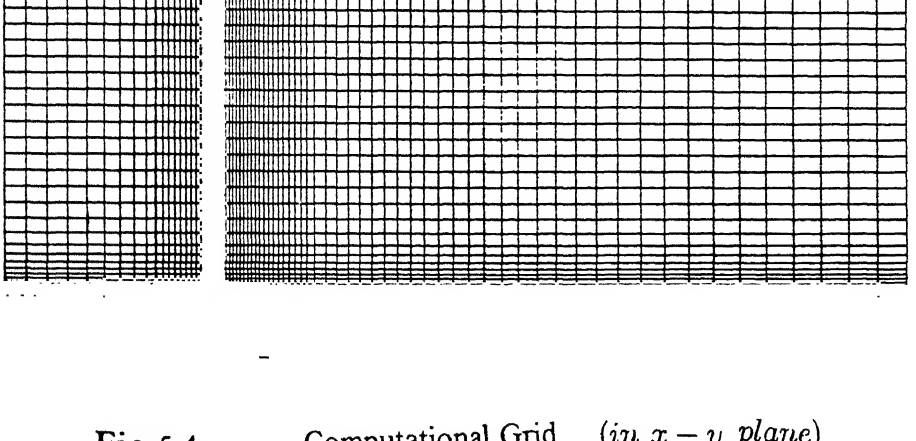

Fig 5.4 Computational Grid *(in $x-y$ plane)*

5.2 THE FLOW AND THE TEMPERATRUE FIELD

The computed velocity field, downstream of a row of holes along the hole centreline plane is presented in Fig. 5.5. Here the effect of turbulence is simulated by using the Baldwin-Lomax model (with built-in relaxation technique) and an exit profile, approximated by a 1/7 power law. Figure 5.5 indicates a strong jet crossflow interaction in the near field region. The velocity profile in this region exhibits two zones namely (a) the momentum deficit zone indicating the development of a shear layer between the inner layer of the injected jet and the crossflow, and (b) the region right above the momentum deficit zone, with a slight velocity over shoot caused by the accelerating cross flow. Figure 5.6 indicates the velocity field on the x-z plane at a horizontal cross-section very near to the surface. This figure shows that, the region beneath the jet is ventilated by the mainstream sideways and therefore a low effectiveness may occur just at the immediate downstream of the injection. At this angle of injection there is no sign of flow separation at the immediate down stream of the hole. A more complex flow structure is observed on the cross-stream planes. The cross-stream velocity vectors are presented in Fig. 5.7. The counter rotating vortices are well captured and the strength of the vortices are prominent upto a X/D of 10. The strength of this counter rotating vortices is reduced than beyond a distance of X/D equal to 15. This indicates that the jet tends to mix with the mainstream and the three dimensionsality is eventually reduced. However along the centre line between any two holes, there is some rolling of fluid and this rolling is even predominent at X/D

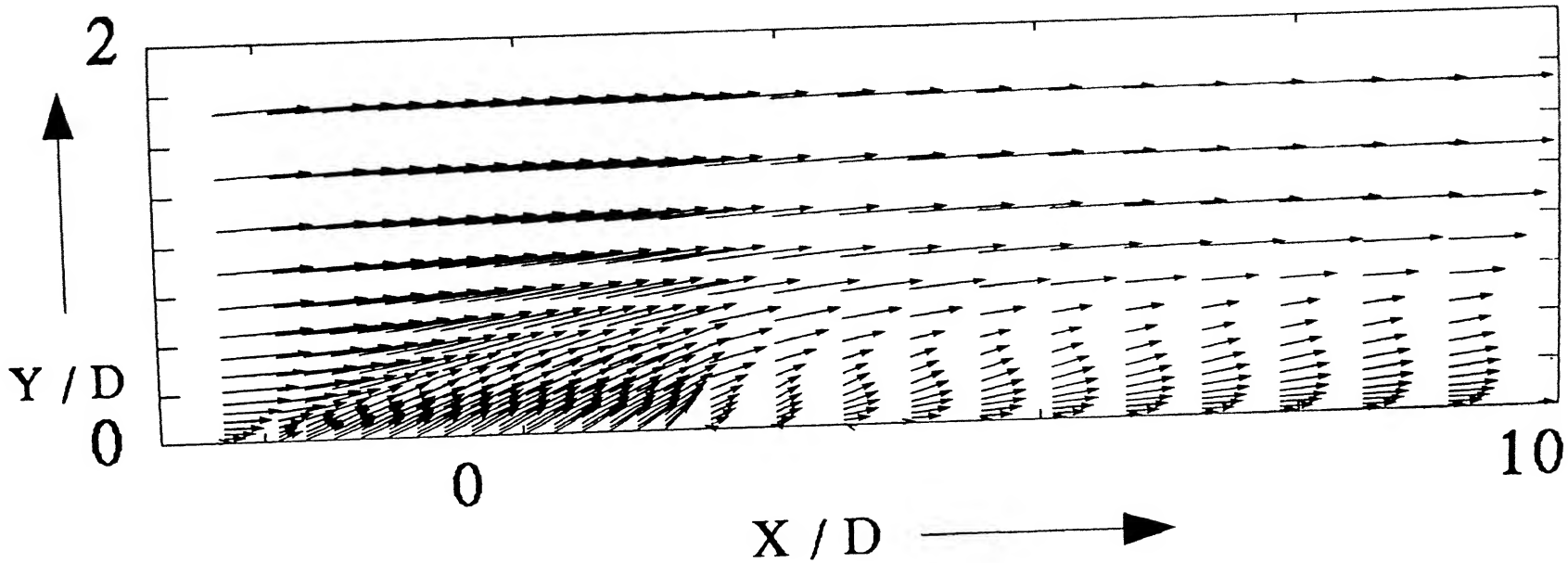

Fig 5.5 Computational centreline velocity profiles down stream of a row of holes

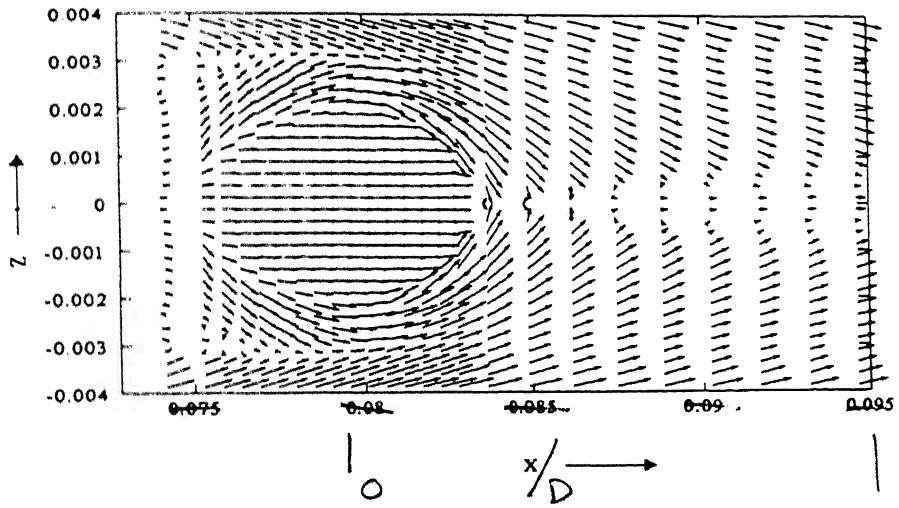

Fig 5.6 Computed velocity profile in x-z plane near the hole .

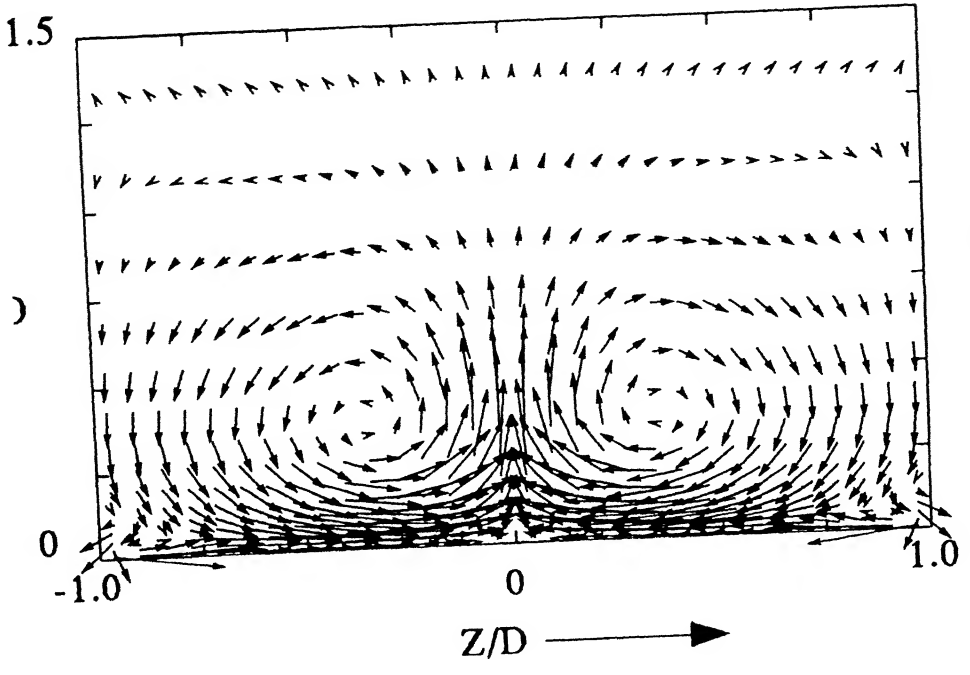

X / D = 5

(a)

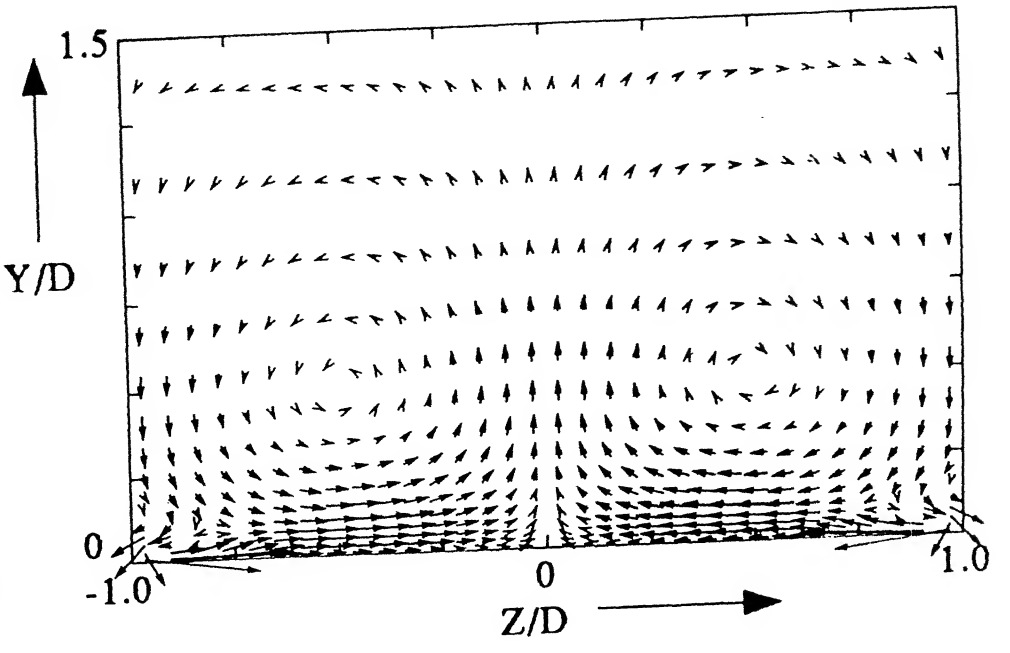

X / D = 10

(b)

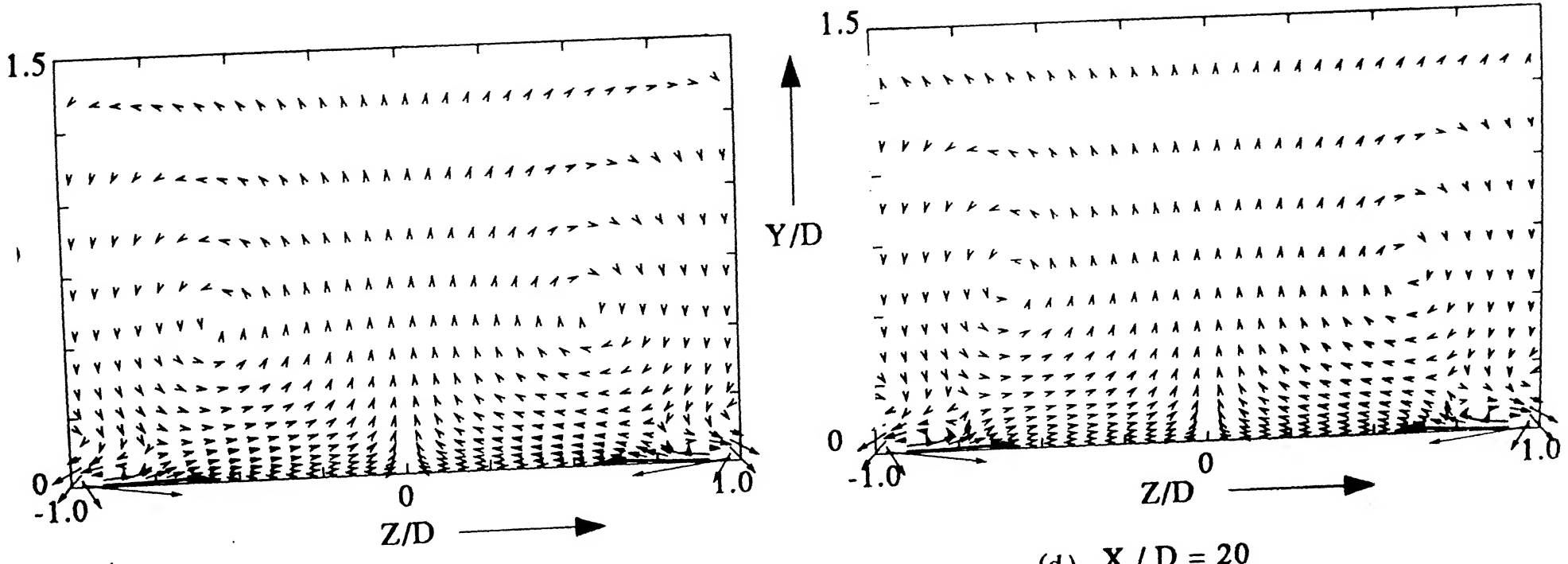

(c) X / D = 15

(d) X / D = 20

Fig 5.7 Velocity vectors in different cross stream planes showing contra-rotating vortices

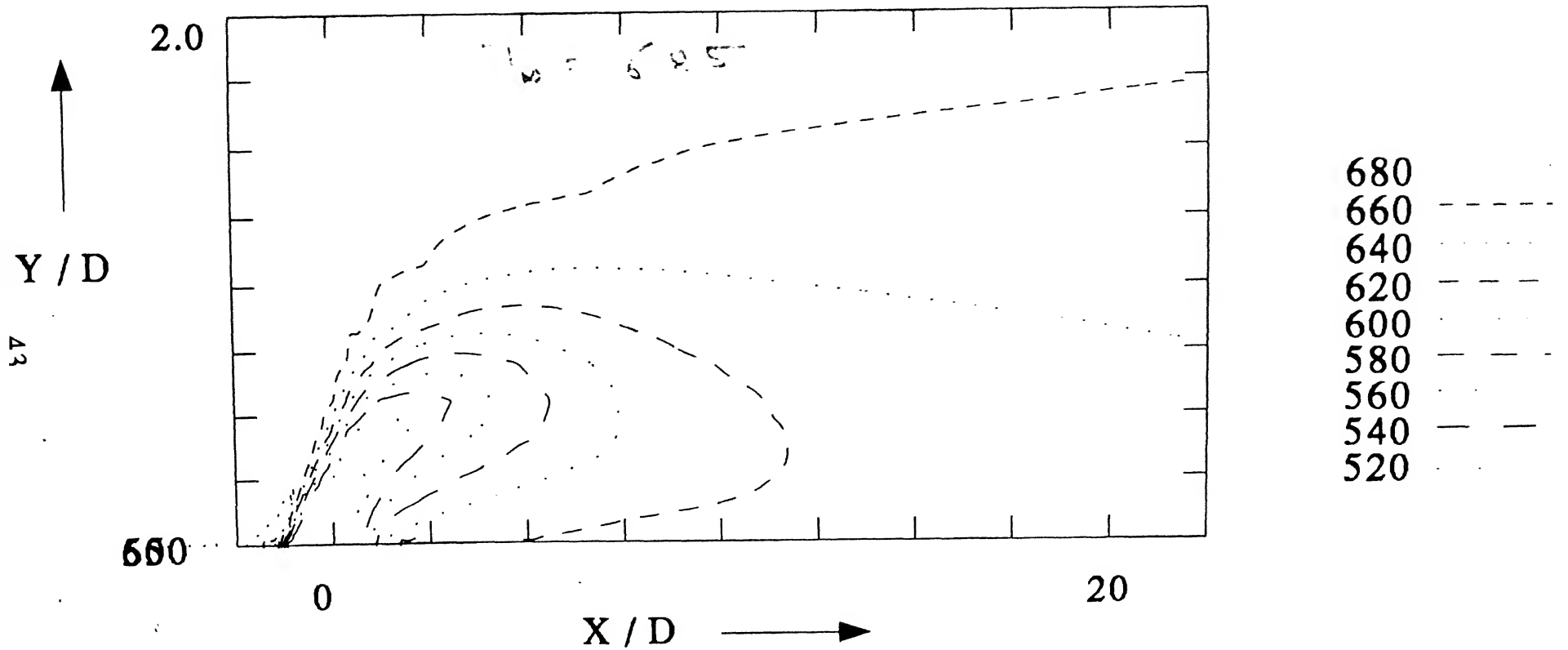

Fig 5.8 Computational centreline temperature contours downstream of a row of holes

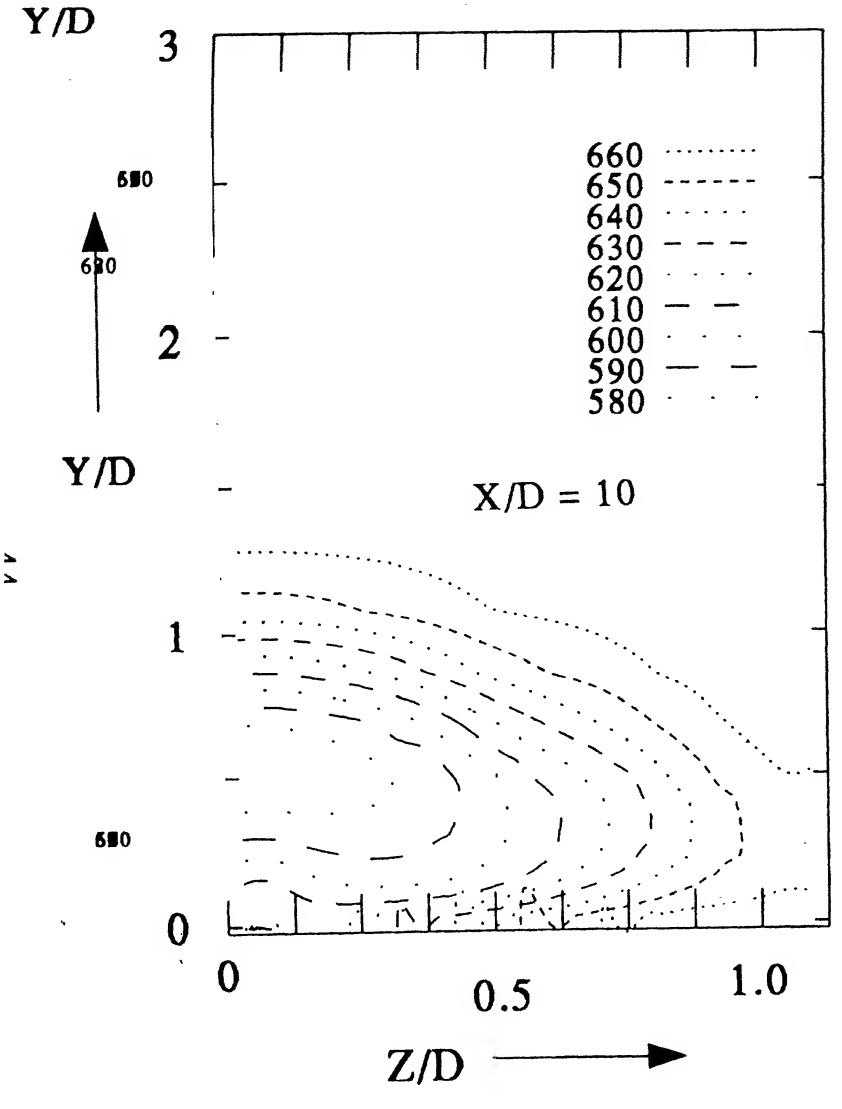
Y/D
3
2
1
0
660
650
640
630
620
610
600
590
580
X/D = 10
0
0.5
1.0
Z/D

(a)

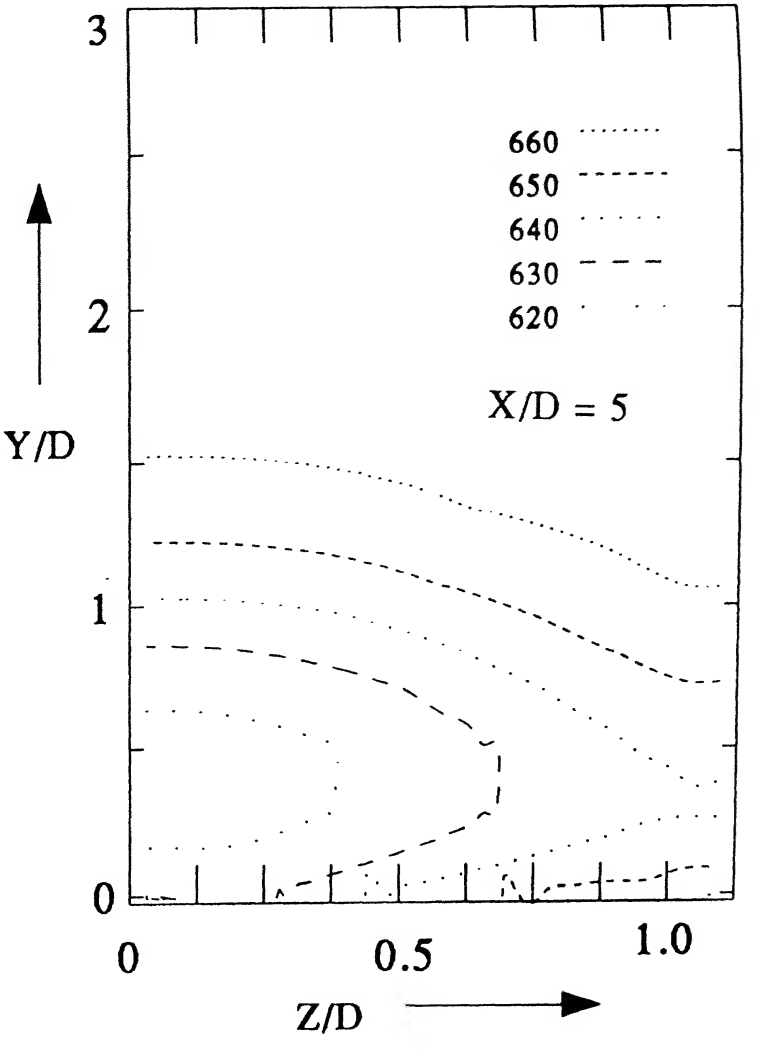
3
2
1
0
660
650
640
630
620
X/D = 5
Y/D
0
0.5
1.0
Z/D

(b)

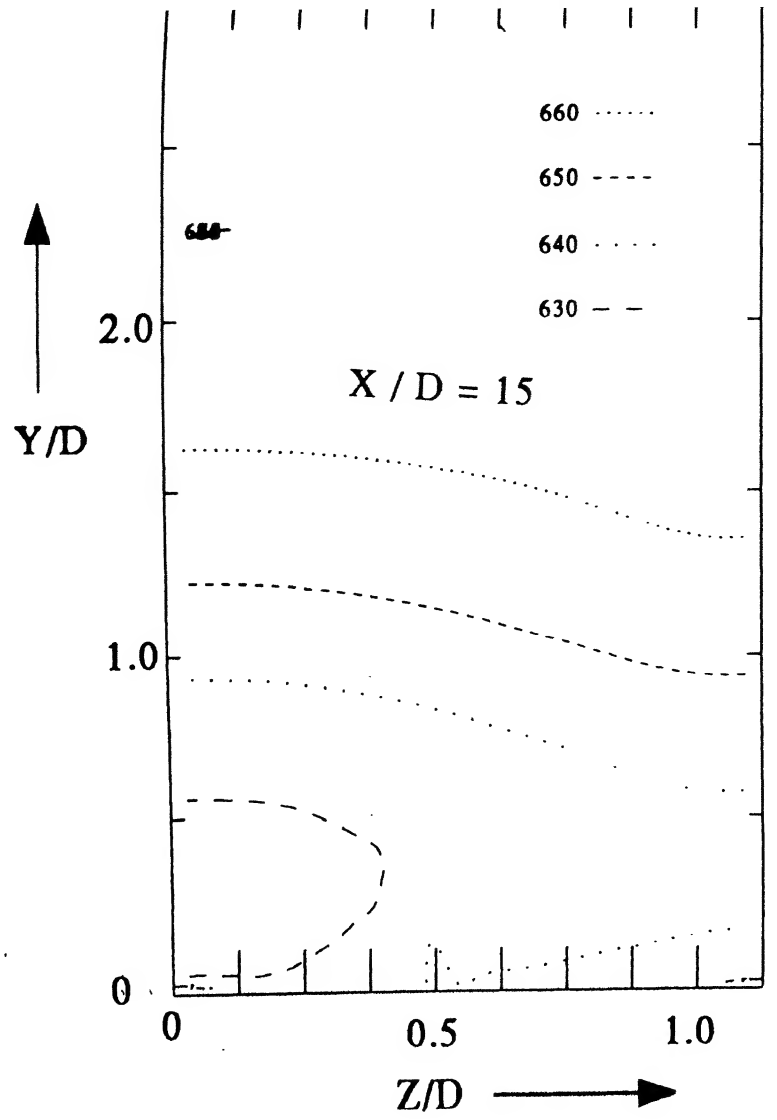

(c)

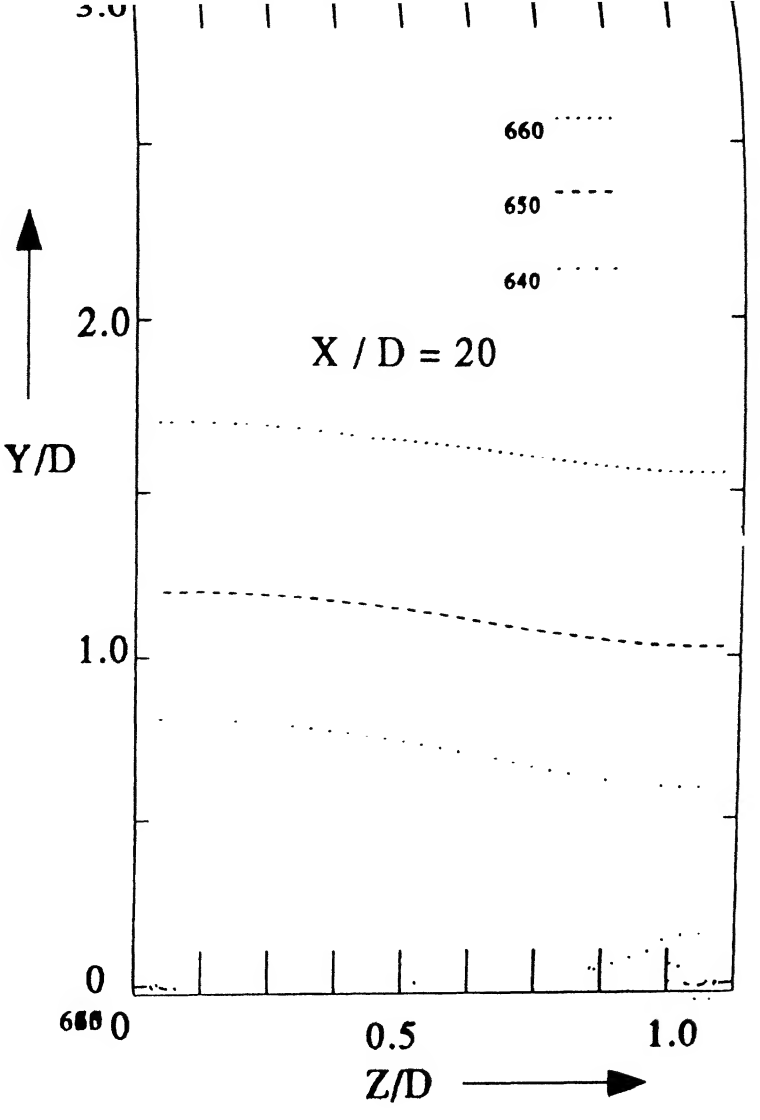

(d)

Fig 5.9 Predicted temperature contours on different cross stream planes indicting the jet trajectory and lateral diffusion

equal to 20. This is what culminates due to the interaction of the coolant layer coming from two sides.

The jet trajectory can also be determined by the temperature field. Figure 5.8 depicts the temperature field on a x-y plane along the centre line of the holes. The non-uniformity in the thermal field is prominent in the near field region with a jet like trajectory. The kidney shaped cross-section of the vortices are well captured through the cross stream temperature contours (Fig. 5.9) for X/D upto 10.0. At a downstream distance of X/D = 20, the three-dimensionality is ceased and the temperature field shows more uniformity (Fig. 5.9(d)).

5.3 ADIABATIC FILM COOLING EFFECTIVENESS

Figure 5.10 shows the predicted film cooling effectiveness (η). The results are compared with the experiments of Schiffer and Hennecke where the exit velocity has been assumed to be uniform. As seen from Fig. 5.10(a), the distribution of film cooling effectiveness along the centre line of the holes compares well with the experimental data in the range of $X/D \geq 15$. However, the effectiveness is underpredicted in the near field of the injection hole ($X/D < 15$). This under prediction may be explained, in light of cross stream ventilation effect. The experimental results do not reveal such behaviour. Figure 5.10(b) illustrates the variation of effectiveness along the centreline between two holes. It is evident that in the far downstream ($X/D \geq 30$), the computational results match the experimental data reasonably well. However in the near - field region, effectivenss is once again underpredicted. Presumably the lateral diffusion of the jet is underpredicted by the present turbulent model. The pointer from the turbuelence literture indicates that the near field region is dominated by anisotrpic turbulence. Any model based on isotropic eddy viscosity

assumption admittedly fails to capture the actual distorsion of strain rates. The above stated fact is more clearly appreciated by the distribution of lateral variations of film cooling effectiveness at different cross-sectional planes in the near-field region (Fig. 5.10(c)) . Figure 5.11(a), (b) and (c) depict the distribution of the film cooling effectiveness onthe plate, at the similar loctions (viz., along the centre line f the holes, along the centre line between the holes and along different cross-stream planes) as seen in Fig. 5.10. The velocity profile of the emanating jet in Fig. 5.11 corresponds to a 1/7 th power law profile. Interestingly, in all the cases, the predicted results corroborate the experimental observations of Pietrytz (1989) in the downstream region. Here the trend is same as previous case.

Figures 5.12(a), (b), and (c) show the comparison between the predicted and experimental results for a polynomial exit velocity profile. The polynomial velocity profile in this case is so chosen that the peak of the profile is shifted towards downstream direction. Such a profile corrosponds to the experimental observation with high blowing ratio. The comparison makes it evident that the polynomial exit velocity profile with a positive shifts fails to simulate a realistic flow situation.

Figure 5.13(a), (b) and (c) show a similar comparison between the experiment and the predictive procedure using a polynomial exit velocity profile with a shift towrads the upstream. It may be mentioned tht this particular situation corresponds to a low blowing ratio. However, the comparison depicts the inability of the simulation in the case of a polynomial exit velocity profile with negative shift (shift towards the upstraeam).

Sarkar and Bose (1995) have observed that the Baldwin Lomax model can predict effectiveness quite well in the far downstream of the injection hole. They also

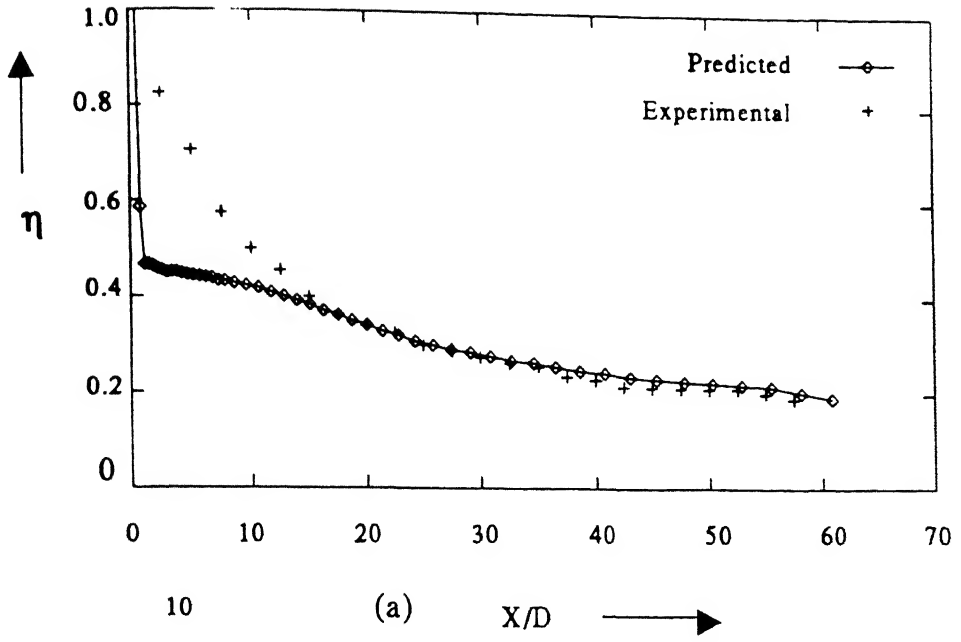

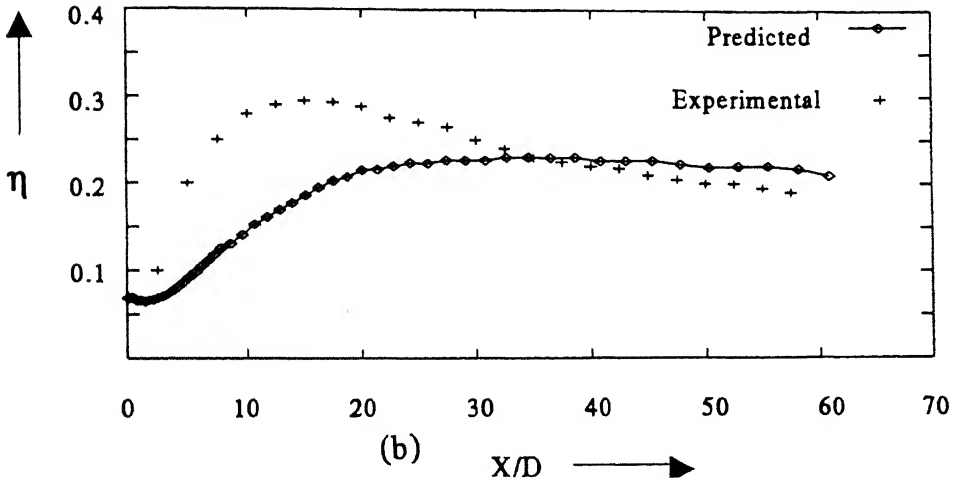

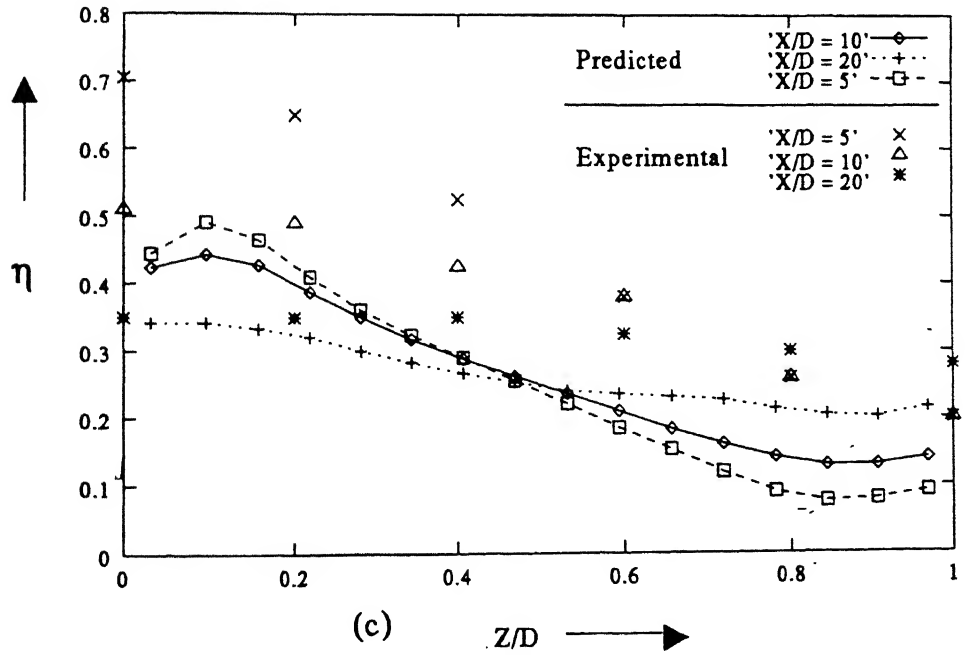

Fig. 5.10 Variation of adiabatic film cooling effectiveness (for

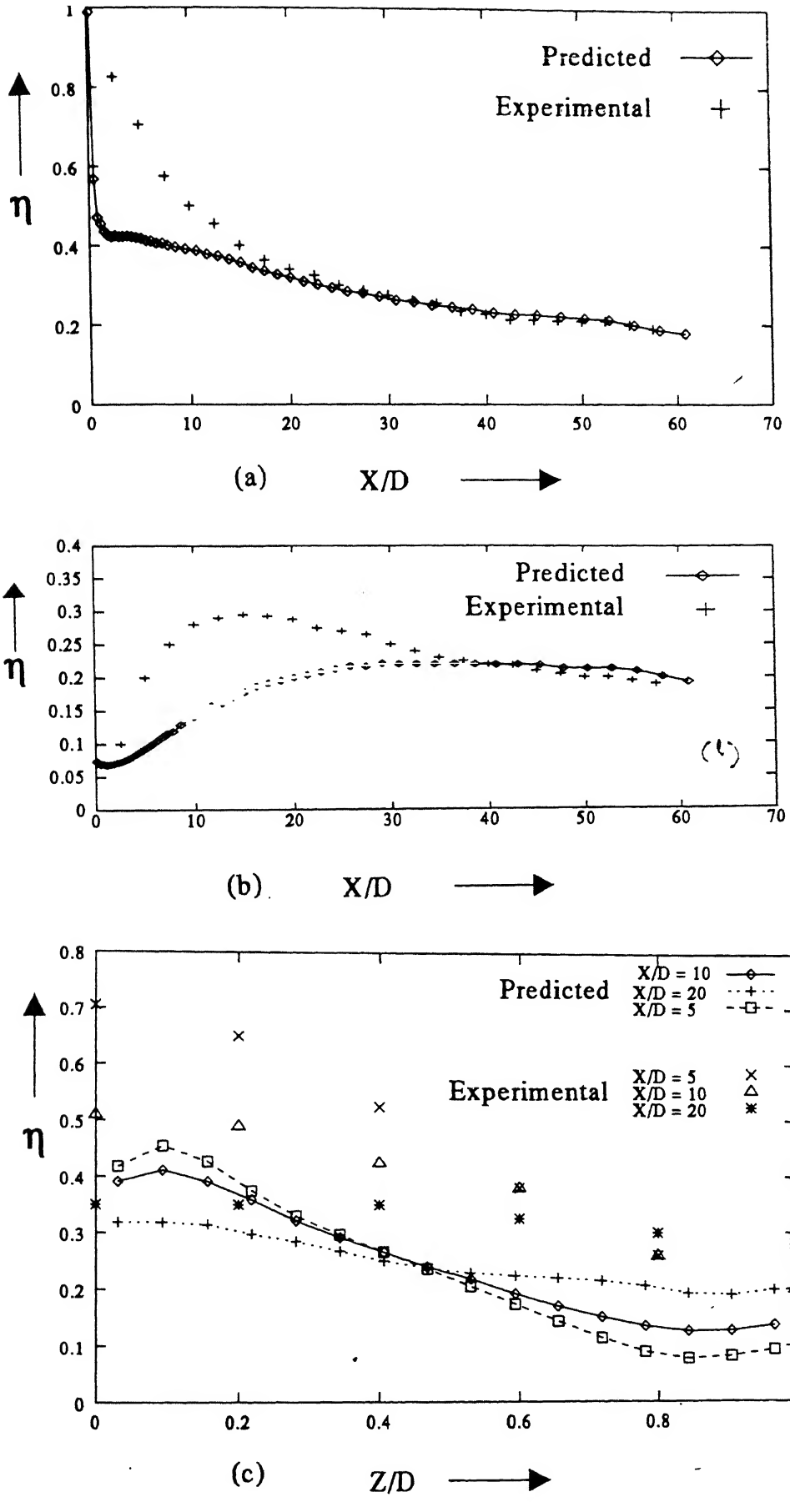

Fig 5.11 Variation of adiabatic film cooling effectiveness (for 1/7 power law hole exit profile)

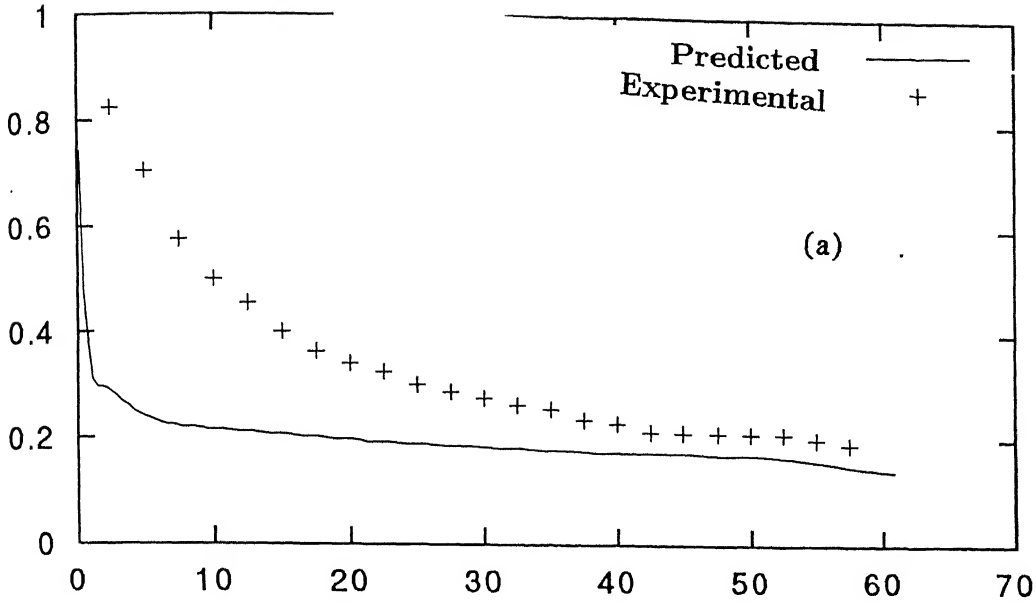

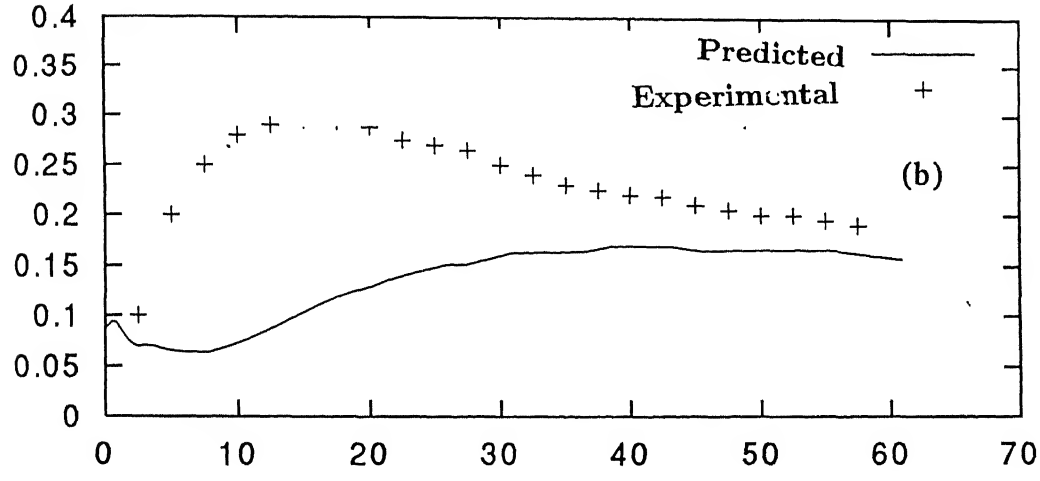

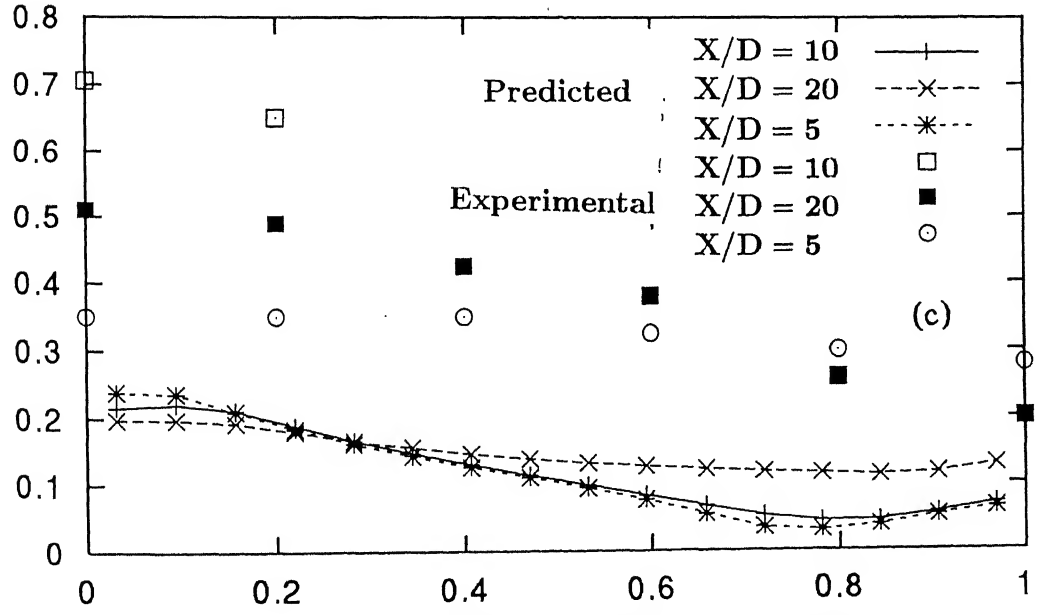

Fig 5.12 Variation of adiabatic film cooling effectiveness (for polynomial profile hole exit profile with the peak of

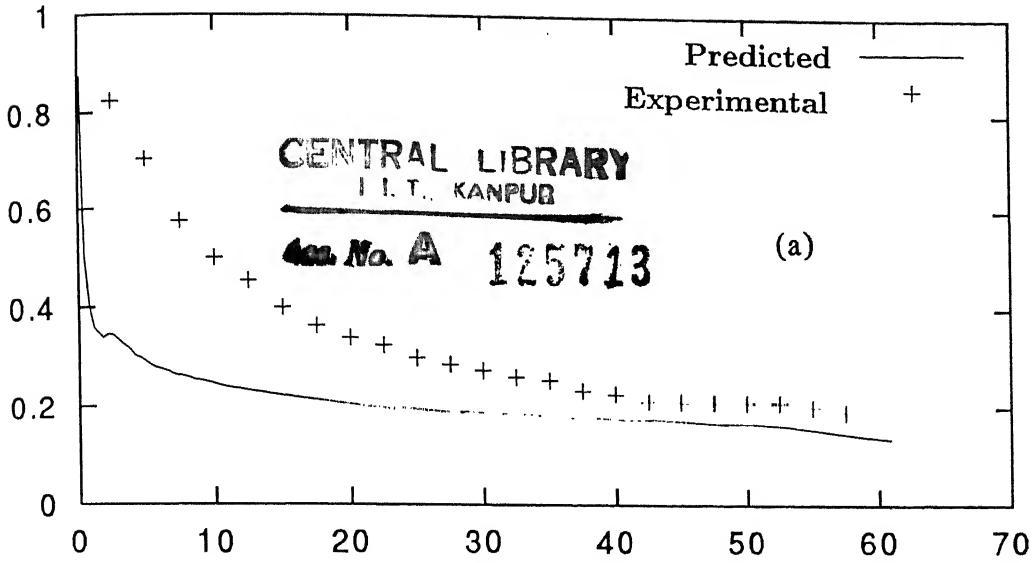

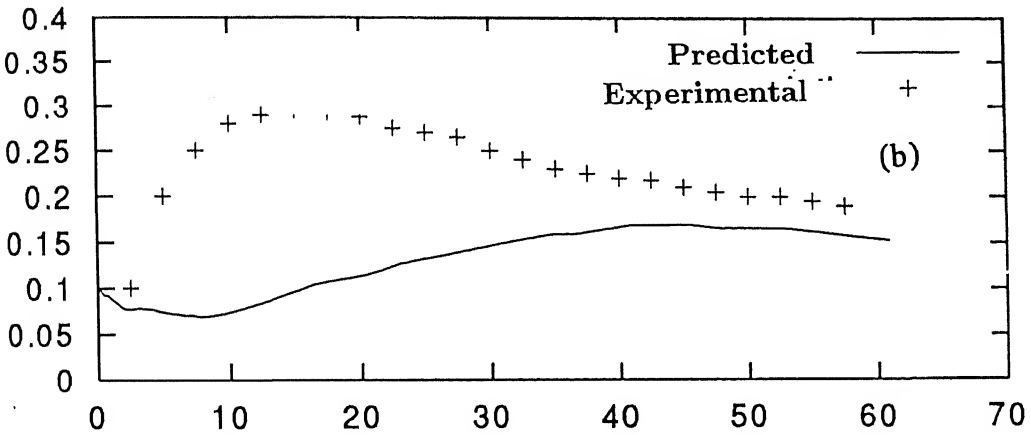

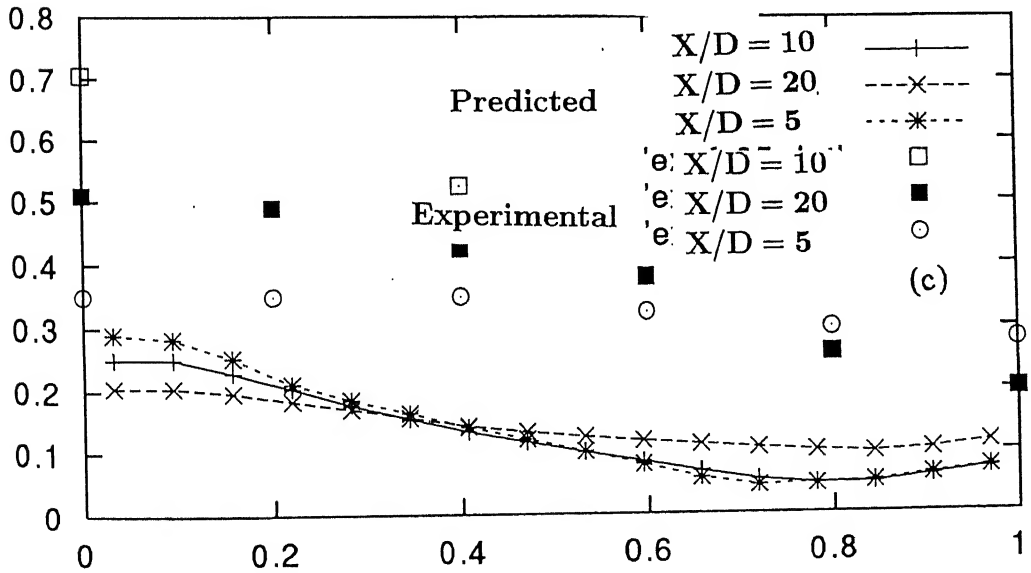

Fig 5.13 Variation of adiabatic film cooling effectiveness (for polynomial profile hole exit profile with the peak of

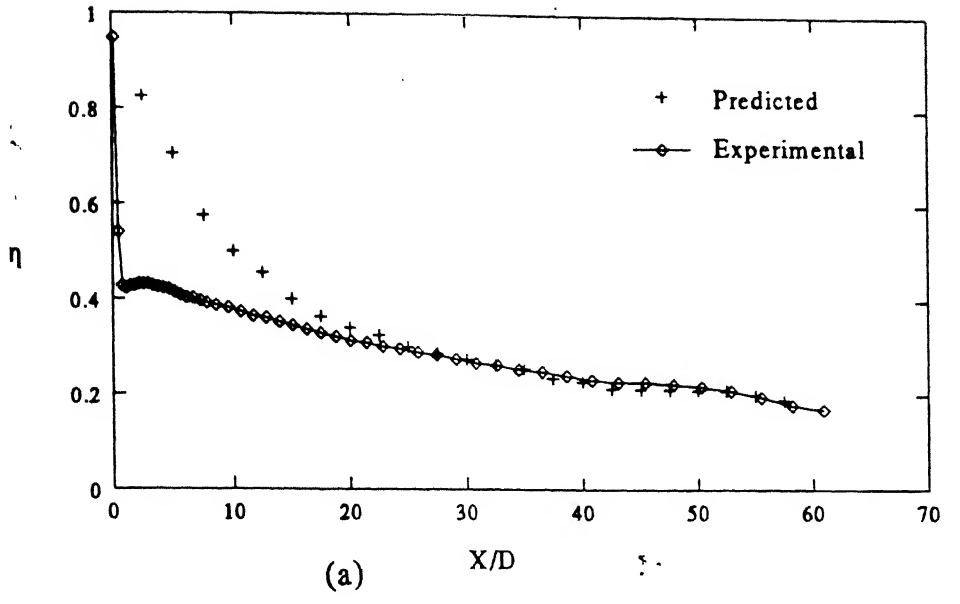

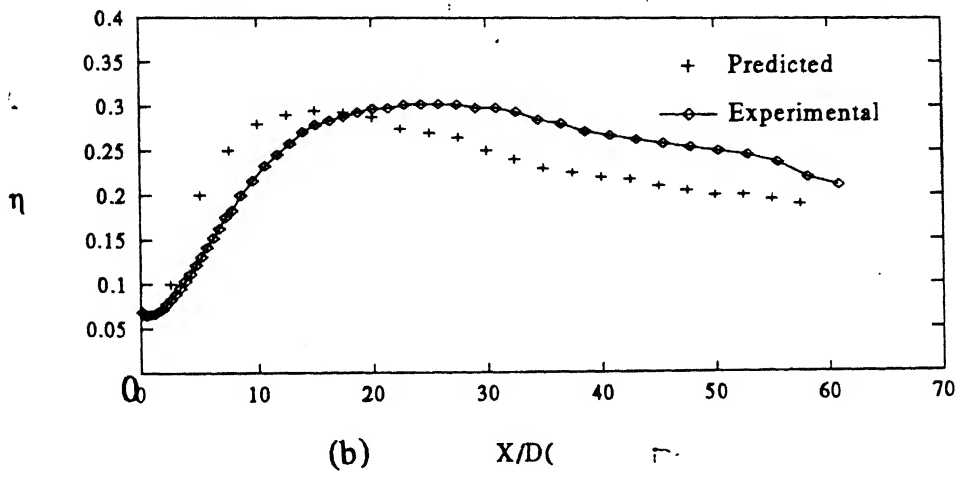

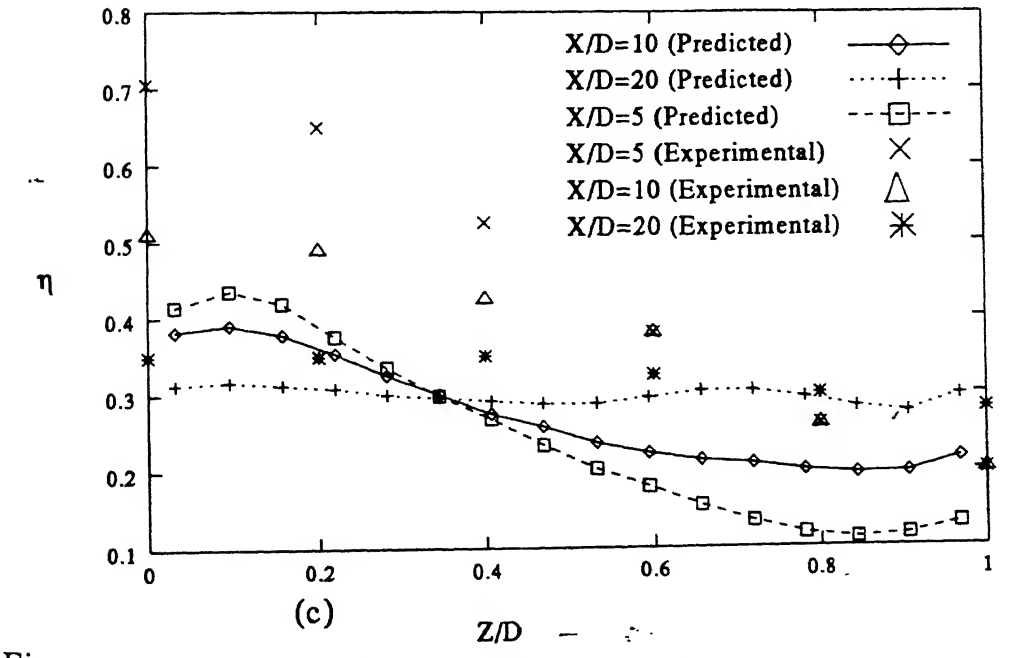

Fig 5.14 Variation of adiabatic film cooling effectiveness (for 1/7 th power law hole exit velocity profile) showing the

found that the prediction did not match well with the experimental results near the injection hole. They indicated that a relaxation model would be appropriate to predict the near hole region. We have made use of the same relaxation model for improvement in the predictive procedure. Figure 5.14 (a), (b) and (c) show the distribution of predicted effectiveness due to the aboe mentioned relaxation model on the plate at different locations. The predicted results reveal a highly encouraging comparison with their experimental counterpart. Figure 5.14(a) illustrates that the predicted effectiveness along the hole centreline is very close to the experimental results for X/D greater than 20. However no appreciable improvement is discerned in the prediction of hole centreline effectiveness near the injection hole. Figur 5.14(b) shows the distriburtion of effectiveness along the line between two successibe holes. The values of predicted effectiveness are somewhat improved near the injection hole. Figure 5.14(c) shows the lateral variation of the effectiveness at various cross-stream locations. It is clear from this result that the lateral variation of the effectiveness is close to the experimental results at X/D = 20. Some improvement is also brought about at other X/D locations but the extent of improvement is not noteworthy.

5.4 PARAMATRIC STUDY

The jet trajectory which primarily depends on the angle of injection and the momentum ratio ,has a remarkable influence on the film cooling. A high trajectory implies deeper penetration of the jet into the cross flow, pronounced flow mixing and hence less effectiveness. On the other hand low trajectory results in an attached coolant layer, less mixing and high effectiveness. The influence of the blowing ratio and the angle of injection on the film cooling will be discussed in the following section.

5.4.1 Blowing Ratio

Blowing ratio, as explained earlier is the ratio of mass flow rate of the coolant to the mainstream flow. Figure. 5.15 shows the variation of effectiveness for three different blowing ratios. The angle of injection has been taken as 30°. It is clear that the effectivness along the hole centre line (Fig. 5.15 (a)) and the effectiveness along the line between two holes (Fig.5.15 (b))are high for low blowing ratios at the near injection region.This trend is gradually altered as the flow travels downstream. The reason may be attributed to the high penetration of jets into the crossflow and more sideway ventilation of mainstream as blowing ratio is increased. However, in the far down stream, the film formation takes place and the effectiveness improves. Fig 5.16 shows the temperature contours in the streamwise direction for two different blowing ratios.

5.4.2 Angle of Injection

Figure 5.17 (a) and (b) show the variation of effectivenes for three different angles of injection. The results are obtained for $\alpha = 30°$, 60° and 90° with the blowing ratio of 0.559. It can be discerned from Figure 5.17(a) that the effectiveness is high for the low angles of injection near the injection hole. Whereas for the high angles of injection, the effectiveness low owing to the side ventilation effect. It is also clear

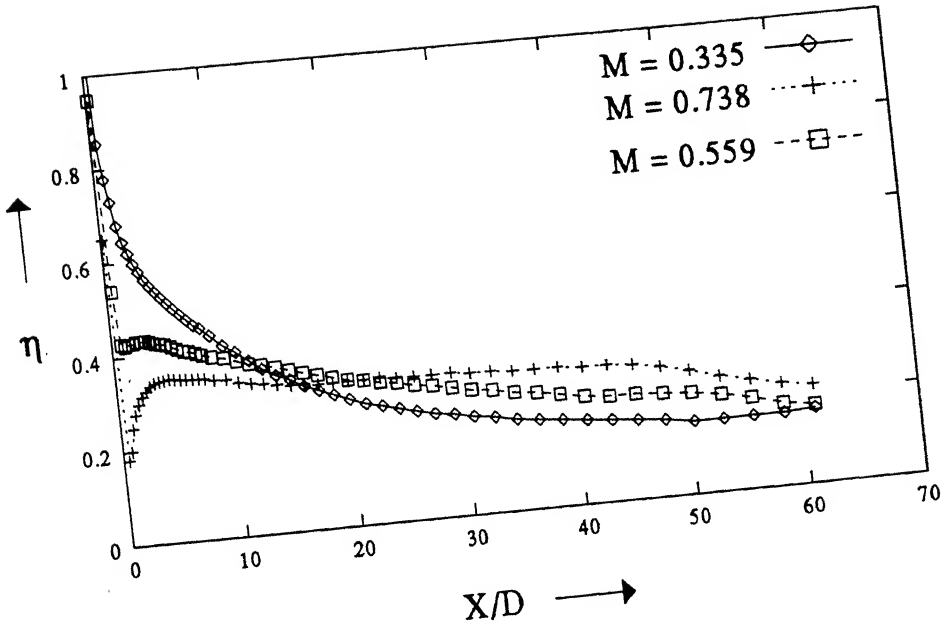

Fig. (a)

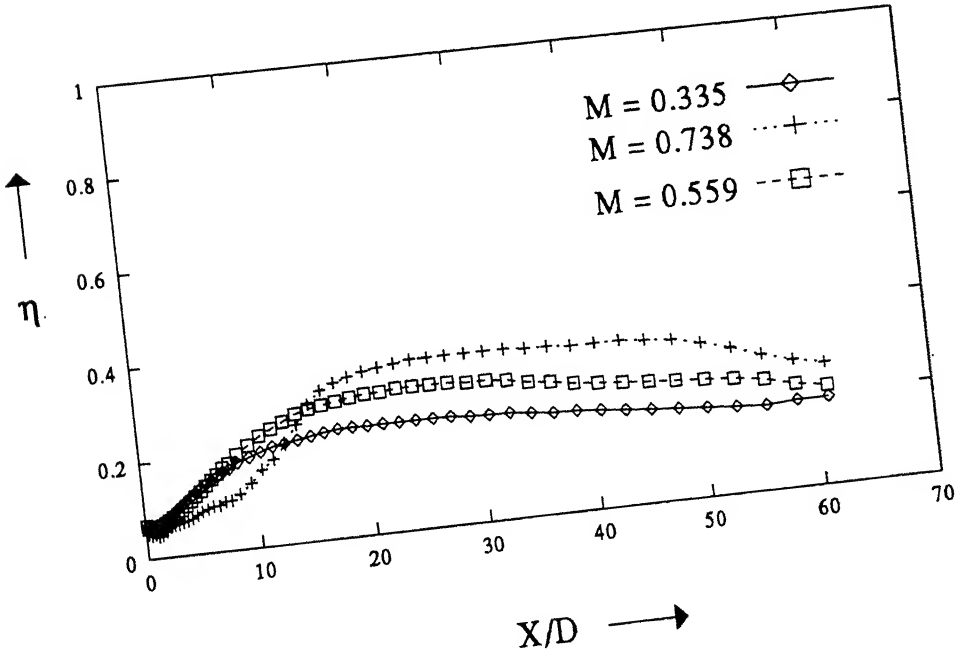

Fig. (b)

Fig 5.15 Variation of adiabatic film cooling effectiveness for three different blowing ratios

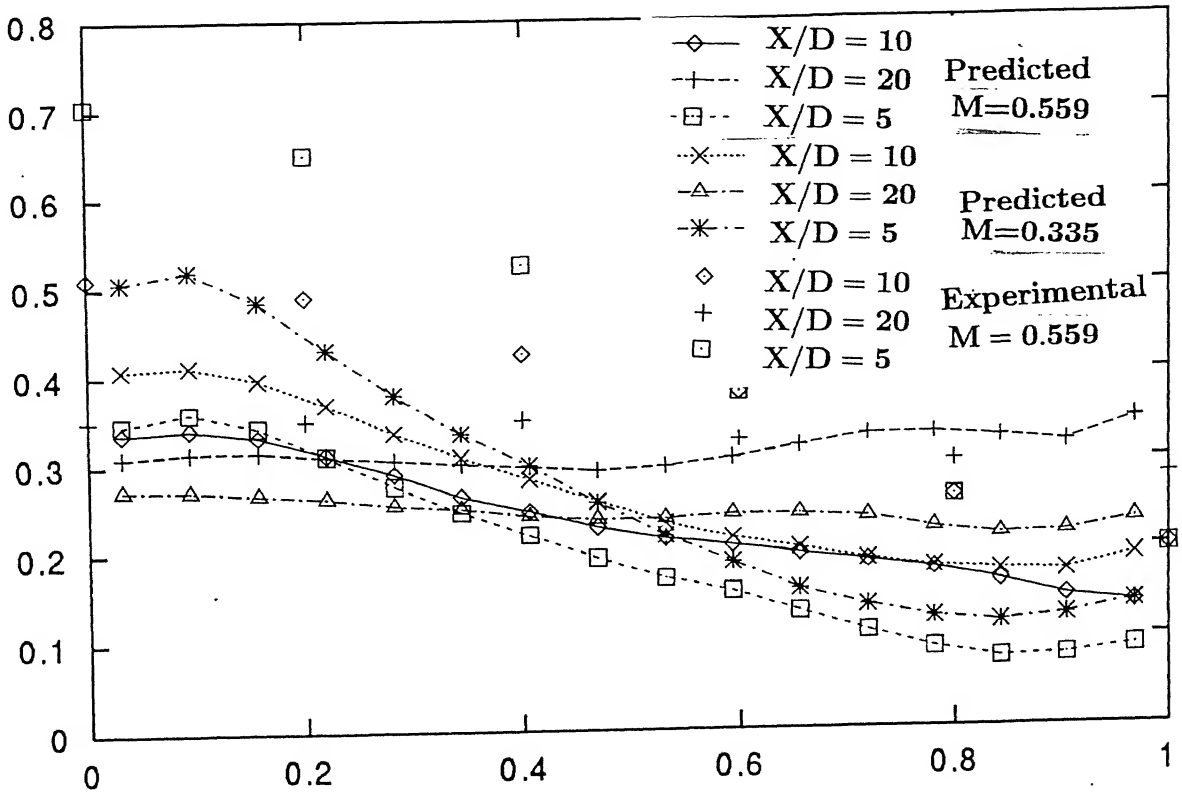

Fig 5.16 Variation of adiabatic film cooling effectiveness for three different blowing ratios at various cross stream planes

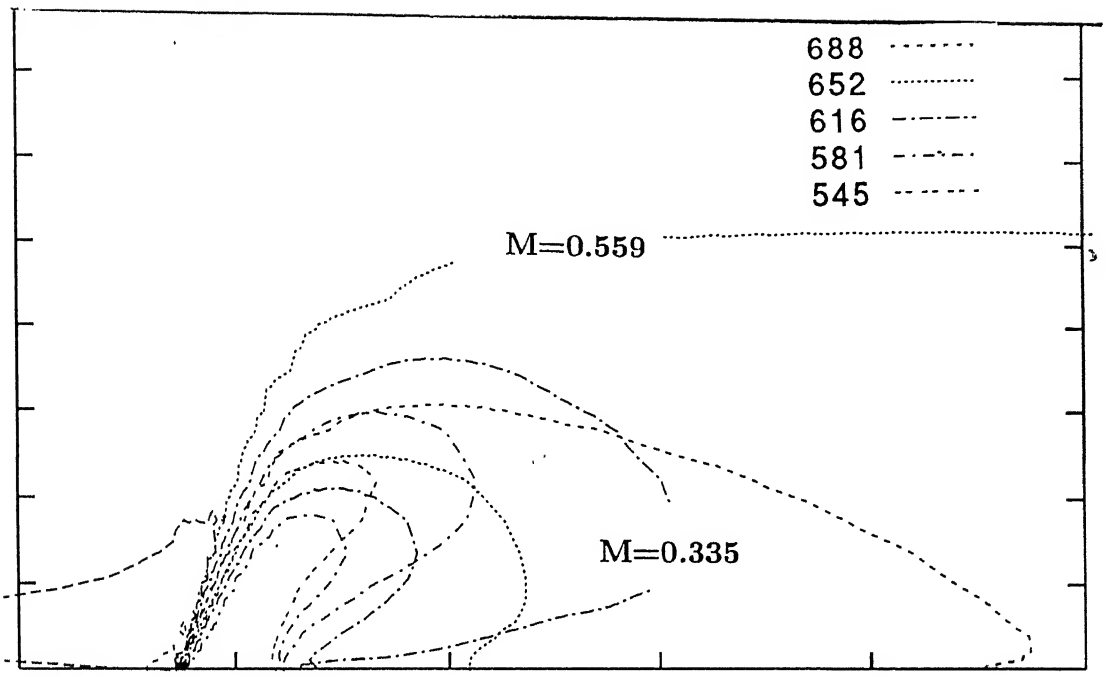

Fig 5.17 Computational centreline temperature contour downstream of a row of holes for two different blowing ratios

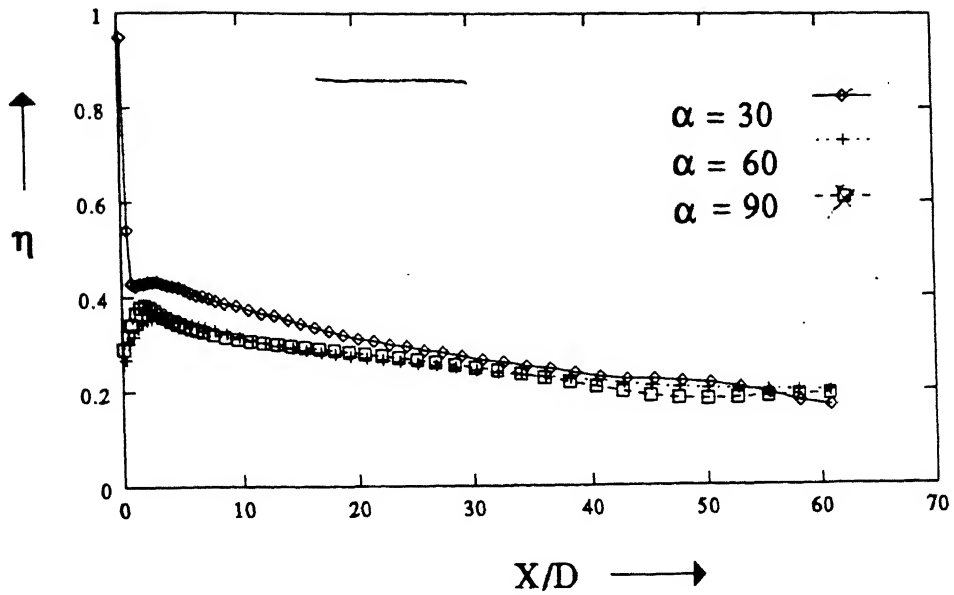

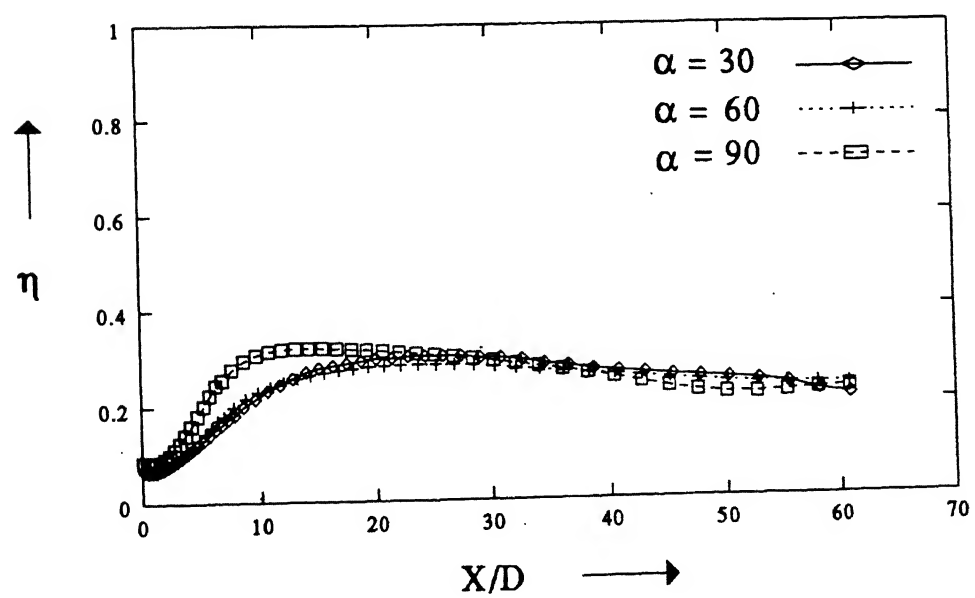

Fig 5.18 Variation of adiabatic film cooling effectiveness for three different angles o injection

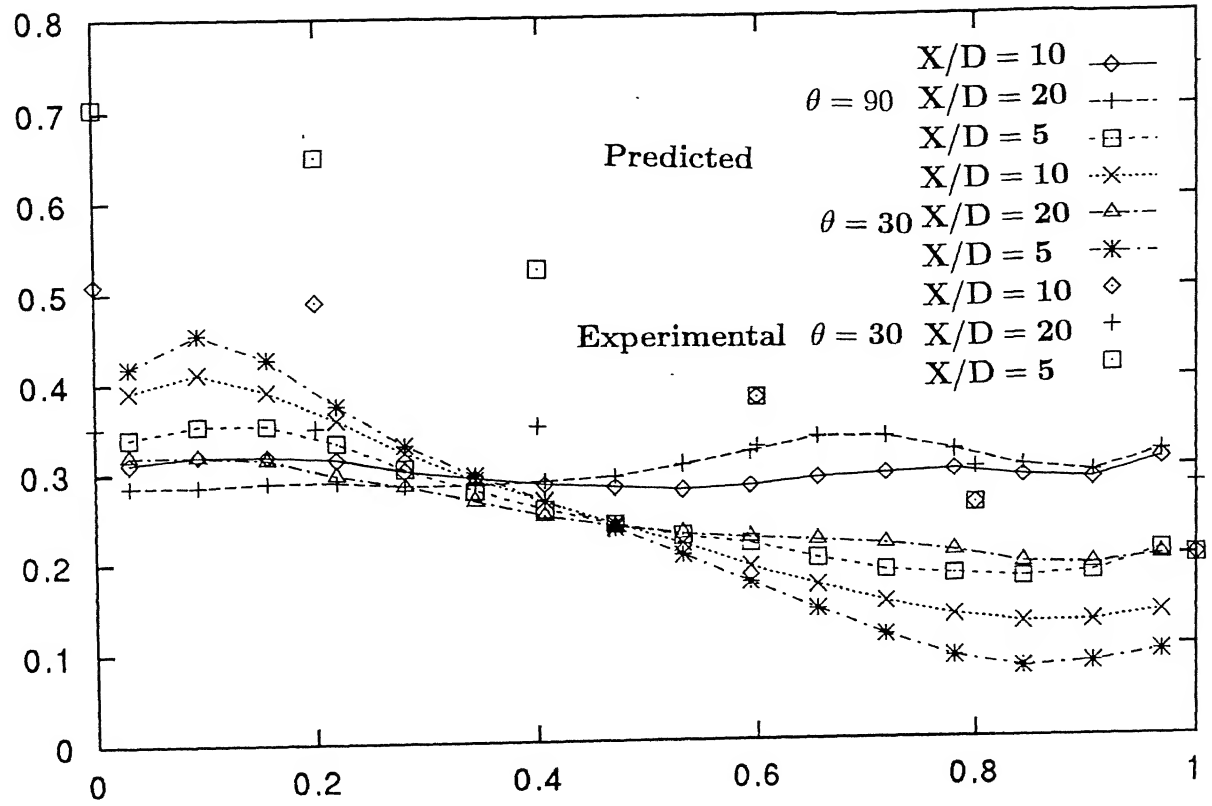

Fig 5.19 Variation of adiabatic film cooling effectiveness for two different angles of injection at various cross-stream planes

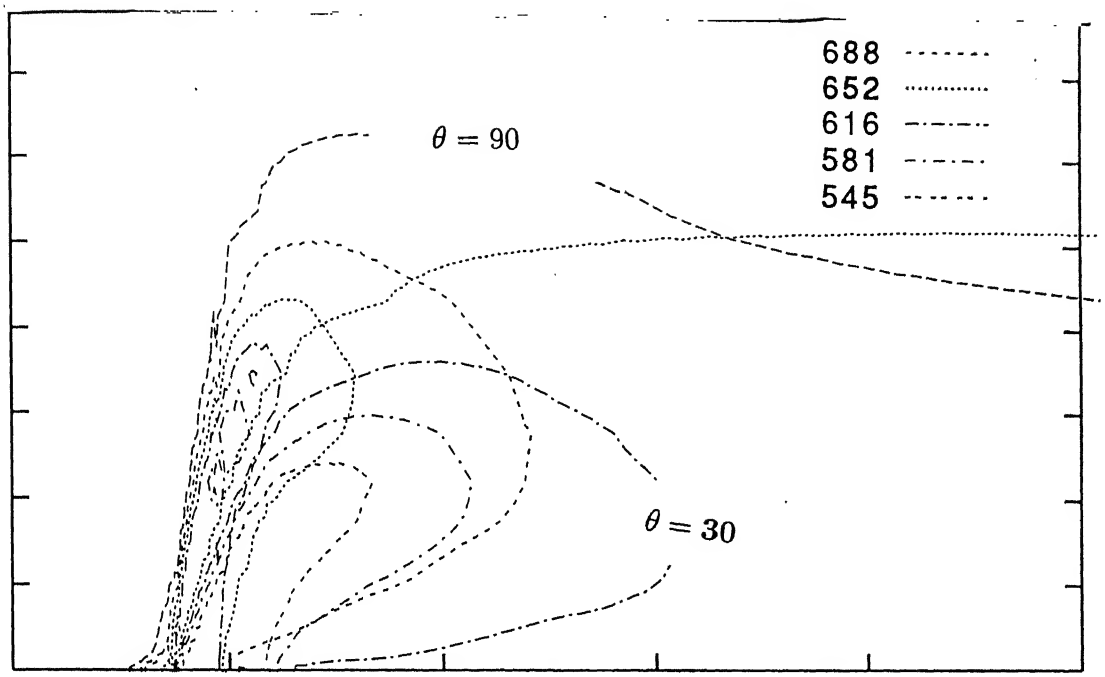

Fig 5.20 Computational centreline temperature contour, downstream of a row of holes for two different angles of injection.

that the effectiveness in the downstream is almost uniform for high angles of injection. The effectiveness along the centerline between the holes is high near the hole for the high angles of injection and in the downstream the effectiveness ceases to be a function of angle of injection (Fig 5.17 (b)).

For the high angle of injection, the effectiveness drops immediately after the injection to a minimum and increase again followed by a gradual drop. This behaviour can be explained by the jet lift off mechanism. The jet penetrates into the mainstream and the region beneath the jet is ventilated by the mainstream resulting in immediate drop of effectiveness at the immediate downstream of the injection holes. After a short distance, the coolant fluid reaches the wall due to turbulent diffusion and thus the cooling effectiveness increases. In the case of low angle of injection, the effectiveness increases near the injection hole due to the low jet trajectory. Increase in angle of injection leads to a higher jet trajectory, but the jets mixes more rapidly with the main stream than that for low injection angles. Figure 5.18 illustrates that the effectiveness is almost uniform due to $\alpha = 90°$ at X/D = 10. Hence it can be said that at the higher injection angles, uniform lateral spreading is achieved at a shorter down stream distance from the injection hole.

Chapter 6

CONCLUSIONS

Film cooling is one of the most efficient means of protecting the turbine blades from the direct impingement of the hot gas in the gas turbines. The present numerical investigation is devoted towards an in-depth understanding of the coolant behavior and its interaction with the mainstream flow. The study has been confined to cooling of a flat plate. Albeit being an approximate one. the study identifies the relative importance and influence of the governing parameters involved in film cooling. The effect of turbulence has been invoked by an algebraic model. The present formulation is based on the well known Baldwin-Lomax model of turbulence. The modification has been incorporated to bring about the $History Effects$ of turbulence quantifies. The effect of coolant velocity profile at the hole exit. the blowing ratio and the angle of injection on the effectiveness of cooling has been studied for a wide range of parametric variations. The effectiveness corresponding to the 1/7th power law profile compare favorably with the available experimental results.

REFERENCES

Amer, A.A., Jubra, B.A., and Hamdan, M.A.; 1992"Comparision of Different Two equation Turbulence Models for Predition of Film Cooling from two rows of Holes", Numerical Heat Transfer, Part A, 21, 143-162.

Bergeles, G., Gosman, A.D. and Launder, B.E., 1978, "The Turbulent jet in a Cross-stream at low injection rates: A Three dimensional Numerical Treatment: Numerical Treatment". Numerical Heat Transfer, 1, 217-242.

Baldwin, B.S. and Lomax, H., 1978, "Thin layer Approximation and Algebraic Model for Seperated Turbulent Flows:, AIAA Paper 78-257, 1-8.

Cebeci, T., and Smith A.M.O., 1974, "Analysis of Turbuelent Boundary Layers", Academic press.

Crawford, M.E., Kays, W.M. and Moffat, R.J., 1980, "Full Coverage Film Cooling, Part II: Heat Transfer Data and Numericl Simulation", ASME Journal of Engineering for Power, 102, 1006-1012.

Demuren, A.D., Rodi, W. and Schomung, B., 1986, "Systematic Study of Film Cooling with a Three - Dimensional Calcualtion Procedure", Journal of Turbomachinary 108, 124-130.

Favre, A., 1965, " Equations des Gaz Turbulents Compressible: Foster, N.W., and Lampard, D., 1980". The flow and Film cooling Effectiveness Following Injection Through a Row of Holes", ASME Journal of Eng. for Power, 102, 584-588.

Goldstein, R.J., 1971, "Film Cooling", Advnces in Heat Transfer, Academic Press, New York and London, 7, 321-379.

Kayes, W.M., 1966, Convective Heat and Mass Transfer, McGraw-Hill.

Garg, V.K., and Gaugler, R.E., 1997, "Effect of velocity and Temperature Distribution at the Hole Exit on Film Cooling of Turbine Blades", 119, 343-351.

Garg, V.K. and Ameri., Ali A., 1997, "Comparison of two Euation Turbulence Models for Prediction of Heat Transfer on Film Cooled Turbine Blades", Numerical Heat Transfer, Part A, 31; 347-371.

Kim, S.W., and Benson, T.J., "Calculation of a circular jet is cross-flow with a multiple-time-scale turbulence model", Int. J. Heat and Mass Transfer, Vol. 35, No. 10, 2357-2365, 1992.

Leylek, J.H. and Zerkle, R.D., 1994, "Discrete-Jet Film Cooling : A Comparison of Computational Results with Experiments", ASME Journal of Turbomachinery, 116, 358-368.

Mac Cormack, R.W. and Paullay, A.J., 1972, "Computational Efficiencys Achieved by Time Splitting of Finite Differnece Operators", AIAA Paper No. 72-154.

Pietrzyk, J. R., Bogard, D.G., and Crawford, M.E., 1989, "Hydrodynamics Measurements of jet in cross flow for Gas turbine Film cooling Applications", ASME Journal fo Turbomachinery, 11, 139-145.

Sarkar, S. and Lakshmanan, B., 1991,"Applicaiton of Reynolds Stress Turbulence Model to the Compressible Shear Layer", AIAA Journal, 29(5), 743-749.

Sarkar, S., Bose, T.K., 1995, "Numerical Simultion of a 2D-jet Crossflow interaction related to film cooling applications: Effect of blowing rate, injection angle and free-stream turbulence, Sadhana, Vol. 20, part 6, 915-935.

Sarkar, S., Bose, T.K.; 1995, "Comparison differnt Turbulence Modes for Prediction of Slot-Film Cooling: Flow and Temperature Field', Numerical Heat Transfer,

Sarkar, S. and Bose, T.K., 1997, "Numerical Study of Film Cooling: A Three dimensional Calculation" Journal of Energy, Heat and Mass Transfer, 19, 199-206.

Sciffer, H.P. and Hennacke, D.K., 199 , "The Influence of Gas Temperature on Turbine blade film cooling Effectiveness Dtermined with Model Testing", Third European Propulsion Forum, ONERA, Paris.

Sinha, A.K., Bogard, D.G. and Crawford, M.E., 1990, "Film Cooling Effectiveness of a Single row of holes with variable density ratio", ASME paper No. 90-GT-43.

While, F.M., 1974. "Viscous Fluid Flow", McGraw-Hill, New York.

Schonung, B., Rodi, W., "Prediction of film Cooling by a Row of holes with a Two dimensional Boundary Layer Procedure", Journal of Turbomechinery, Vol. 109, 579-587.

Sarkar, S. and Bose, T.K. , 1995, "Navier - Stokes analysis applied to Turbine Cascades", Numerical Methods in laminar turbulent - flow, 881 - 886.

Sarkar, S. , 1997, " A Navier - Stokes Solver for Turbomachinary Film Cooling". Int. Conference on Advances in Mechanocal & Industrial Ingineering.